Breaking Waves in Deep and Intermediate Waters

Marc Perlin,[1] Wooyoung Choi,[2,3] and Zhigang Tian[3]

[1] Department of Naval Architecture and Marine Engineering, and Department of Mechanical Engineering, University of Michigan, Ann Arbor, Michigan 48109-2145;
email: perlin@umich.edu

[2] Department of Mathematical Sciences, Center for Applied Mathematics and Statistics, New Jersey Institute of Technology, Newark, New Jersey 07102-1982

[3] Division of Ocean Systems Engineering, Korea Advanced Institute of Science and Technology, Daejeon, 305-701 Republic of Korea

Keywords

surface wave breaking, energy dissipation, onset prediction, geometric properties

Abstract

Since time immemorial, surface water waves and their subsequent breaking have been studied. Herein we concentrate on breaking surface waves in deep and intermediate water depths. Progress has been made in several areas, including the prediction of their geometry, breaking onset, and especially energy dissipation. Recent progress in the study of geometric properties has evolved such that we can identify possible connections between crest geometry and energy dissipation and its rate. Onset prediction based on the local wave-energy growth rate appears robust, consistent with experiments, although the application of criteria in phase-resolving, deterministic prediction may be limited as calculation of the diagnostic parameter is nontrivial. Parameterization of the dissipation rate has benefited greatly from synergistic field and laboratory investigations, and relationships among the dynamics, kinematics, and the parameterization of the dynamics using geometric properties are now available. Field efforts continue, and although progress has been made, consensus among researchers is limited, in part because of the relatively few studies. Although direct numerical simulations of breaking waves are not yet a viable option, simpler models (e.g., implementation of an eddy viscosity model) have yielded positive results, particularly with regard to energy dissipation.

1. INTRODUCTION

Since the scientific study of water waves began, wave breaking has been of particular interest. Because of its importance with regard to upper-ocean dynamics and air-sea interactions, and hence its possible relation to climate change, wave breaking in deep and intermediate water depths has received much recent attention. Perhaps the papers responsible for precipitating much work over the past 20 years are those of Melville (1982), titled "The Instability and Breaking of Deep-Water Waves," and those of Duncan (1981, 1983), who investigated the breaking waves created by a hydrofoil and the resistance of a hydrofoil that generated the breaking. Melville found two distinct regimes: One concerned the two-dimensional (2D) Benjamin-Feir instability (Benjamin & Feir 1967), and the other was a 3D instability that dominated the former for larger values of wave steepness, *ka*, and agreed with the results of McLean et al. (1981). Conversely, Duncan's investigations, although generated by a hydrofoil, established and discussed a breaking strength parameter that partially forms the basis for much of the discussion herein.

In the two decades that followed Duncan's and Melville's papers, in addition to several relevant articles on the topic, including the laboratory study by Rapp & Melville (1990) that provided remarkable insight on wave breaking, five important *Annual Review of Fluid Mechanics* articles were published with regard to breaking waves, and we refer the interested reader to them. Banner & Peregrine (1993) presented a comprehensive review of both field measurements and laboratory studies of breaking waves. Secondary effects associated with breaking were discussed as well. Melville (1996) discussed how breaking surface waves affect air-sea interactions and included a useful discussion on the dynamics of breaking waves. Perlin & Schultz (2000) reviewed capillary effects on surface waves and breaking onset and in addition discussed breaking models of forced standing waves. Duncan (2001) reviewed research on spilling breakers and, in particular, his far-reaching contributions to this area, including relevant kinematics. Lastly, Kiger & Duncan (2012) reviewed mechanisms of air entrainment in plunging jets in general and specifically in breaking waves.

In this review article, we organize our discussion around three physics-based areas in which we feel the most progress has been made over the past 20 years: the geometry of breaking, breaking-onset criteria, and dissipation due to breaking. We discuss progress in three dimensions as well as in two dimensions where appropriate. Additionally, as no review of breaking waves can or should ignore field measurements and numerical simulations, we discuss these two topics in some detail. Lastly, we summarize the overall progress toward an understanding of the physical processes associated with breaking waves in deep and intermediate water depths.

2. GEOMETRY OF BREAKING WAVES

2.1. Breaking-Wave Steepness and Crest Asymmetry

For a 2D sinusoidal wave in deep water, its profile is well defined with only two independent parameters, e.g., the wave amplitude (*a*) and wavelength (λ), the quotient of which is an important geometric parameter and from which one can form the wave steepness *ka*. Here $k = 2\pi/\lambda$ is the wave number. As *ka* increases, a gravity wave becomes nonlinear, and its geometry becomes horizontally asymmetric owing to wave-crest steepening and wave-trough flattening. Moreover, as *ka* increases further, the wave also exhibits fore-aft asymmetry because of wave-crest front-face steepening. As *ka* grows to 0.443 (crest angle 120°), according to Stokes' (1880) theory, a limiting condition is reached and wave breaking occurs.

In laboratory experiments, the limiting steepness associated with incipient wave breaking has been examined extensively. Experimental observations show that the limiting steepness is typ-

ically smaller than the Stokes breaking limit. Duncan (1981, 1983) measured the wave height (a_b) and wavelength (λ_b) of steady breaking waves produced by a towed hydrofoil and found that $a_b/\lambda_b \sim 0.1$, which gives a limiting steepness of 0.31. Ramberg & Griffin (1987) observed that the mean of H/gT^2 associated with spilling breakers generated in a convergent channel is 0.021, corresponding to a limiting steepness of 0.41. Here H is the wave height, T is the wave period, and g is the gravitational acceleration. Conversely, incipient wave breaking due to dispersive focusing can occur at a much lower wave steepness, from 0.15 to 0.22 (Rapp & Melville 1990, figure 21), depending on the frequency bandwidth of the wave group. Wu & Yao (2004) generated extreme steep waves due to dispersive focusing and further demonstrated the effects of the spectral bandwidth and shape on the limiting steepness, which decreases approximately from 0.38 to 0.15 as the spectral bandwidth increases from 0.03 to 0.42. Babanin et al. (2010) observed incipient breaking waves due to modulational instability and found that the limiting steepness asymptotically approaches 0.44, although the steepness of individual incipient breakers was approximately 0.40. The variation of the limiting steepness may be related to the different methods of breaking-wave generation and the ambiguity in the definition of incipient breaking waves.

The steepness and surface-elevation profile of spillers and plungers have also been observed to quantify breaking-wave geometry. As wave breaking occurs over length scales from several centimeters to hundreds of meters and waves of the same length scale can break with different intensity (Banner & Peregrine 1993, Melville 1996, Duncan 2001), breaking-wave steepness varies over a large range. For example, Tulin & Waseda (1999, figure 15) found that the steepness of breaking waves due to modulational instability can be in the range 0.22 to 0.41. Tian et al. (2008) observed that local wave steepness immediately before breaking onset ranges from 0.28 to 0.43 for plungers generated by dispersive focusing. Furthermore, Tian et al. (2012) implemented both modulational instability and dispersive focusing to produce breaking waves, the steepnesses of which varied approximately from 0.20 to 0.48. The authors noticed that the steepness of some spillers was considerably higher than that of some plungers, which indicated that the magnitude of wave steepness does not always correlate well with wave-breaking strength.

Other geometric parameters have been sought to represent the geometry of breaking crests. For highly nonlinear gravity waves, sharpened crests and flattened troughs introduce horizontal geometric asymmetry. As waves approach breaking, crest-front faces become very steep, causing vertical geometric asymmetry. Kjeldsen & Myrhaug (1979) and Kjeldsen et al. (1981) introduced the crest-front and -rear steepness (ε and δ, respectively) and the vertical and horizontal asymmetry parameters (β and μ, respectively) to better describe the geometry of breaking crests (**Figure 1**). They reported that the breaking crest-front steepness ranges between 0.32 and 0.78, and the vertical and horizontal asymmetry parameters are as large as 2.0 and 0.9, respectively. Bonmarin (1989) observed breaking-wave profiles at 500 frames per second from a moving carriage. The measured crest-front steepness ε increased from approximately 0.25 to 0.55 within two wave periods prior to breaking onset and reduced to less than 0.20 immediately following breaking (Bonmarin 1989, figure 10). ε at breaking onset correlated with the wave-breaking strength; i.e., averaged values of ε increased from 0.38 for spillers to 0.61 for plungers. Therefore, ε may be more suitable to quantify breaking strength than wave steepness ka. As for the vertical and horizontal asymmetry parameters, it was reported that averaged values of β ranged from 1.20 to 2.14, and averaged μ varied between 0.69 and 0.77, depending on breaking strength. Note that $\varepsilon = \delta = 0.40$, $\beta = 1.0$, and $\mu = 0.61$ for a second-order Stokes wave ($ka = 0.443$) in deep water.

The geometry of 3D breaking waves has been examined in laboratory experiments. She et al. (1994) generated 3D breaking waves using directional focusing and systematically varied the wave convergent angle to examine its effect on the geometry of breaking waves. They found that the breaking crest-front steepness increased from 0.51 to 1.02 as the convergent angle increased (a zero
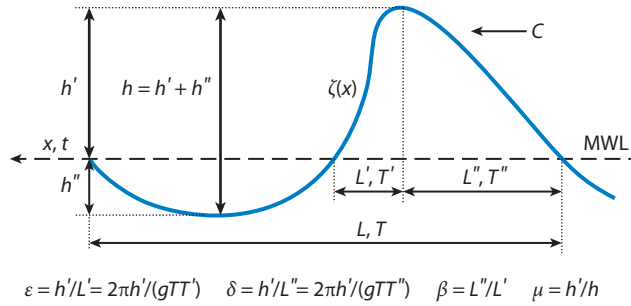
$$\varepsilon = h'/L' = 2\pi h'/(gTT') \quad \delta = h'/L'' = 2\pi h'/(gTT'') \quad \beta = L''/L' \quad \mu = h'/h$$

Figure 1

Definitions of local wave geometry following Kjeldsen & Myrhaug (1979). Abbreviation: MWL, mean water line.

convergent angle corresponds to 2D waves). Alternatively, the horizontal geometric asymmetry parameter, which ranged from 0.65 to 0.67, showed little dependence on the convergent angle. Later, Nepf et al. (1998) examined the breaking crest geometries of 3D waves due to directional spreading, which was achieved by spatially tapering the stroke of individual wave-maker paddles. For such 3D waves, the breaking crest face was steepest ($\varepsilon = 0.52$) in the center, and it monotonically decreased to 0.32 laterally. Conversely, the breaking crest face steepness ($\varepsilon = 0.56$) was laterally uniform for a corresponding 2D breaking crest. Along with the findings in She et al. (1994), Nepf et al. (1998) demonstrated the effect of wave directionality on 3D breaking crests; i.e., the crest-front-face steepness increased from approximately 0.30 to 1.02 as the wave directionality varied from directional spreading through zero angle (2D waves) to directional focusing. Wu & Nepf (2002) further explored the geometry of 3D breaking waves and reported that the crest-front steepness was 0.39 at the onset of 3D spilling breakers due to directional spreading and was 0.41 for that due to directional focusing, compared with 0.38 at the onset for 2D spillers.

It is noteworthy that the determination of the steepness and crest's geometric parameters of breaking waves in laboratory experiments is nontrivial. First, the wave profile close to breaking is highly irregular, which introduces ambiguity in the definition of local wave parameters. Second, breaking waves are highly unsteady, and they deform rapidly. Even with accepted definitions, the timing for the determination of the wave parameters with the spatial measurement of the surface profiles is problematic. Because of the difficulties of spatial surface profile measurements, temporal surface-elevation measurements using wave probes are often utilized to determine wave-steepness and wave-crest asymmetry parameters. However, no straightforward transformation between measurements in the temporal domain and those in the spatial domain is available. Therefore, temporal measurements may not fully represent the spatial characteristics. Yao & Wu (2006) showed that limiting steepness and the crest's geometric parameters of the same incipient breaking waves determined from spatial surface profiles and from temporal surface-elevation measurements are quite different (to 50% variation).

2.2. Wave-Crest Deformation in the Vicinity of Breaking

The wave crest approaching breaking is highly unsteady and deforms rapidly. Initially, measurements of breaking crest deformation were limited to the quantification of wave geometries (e.g., Bonmarin 1989, Rapp & Melville 1990). Observations on the detailed crest-profile evolution of unsteady spilling breakers due to dispersive focusing were essentially nonexistent until the experimental study by Duncan et al. (1994). According to these authors' high-speed (500 fps) imaging
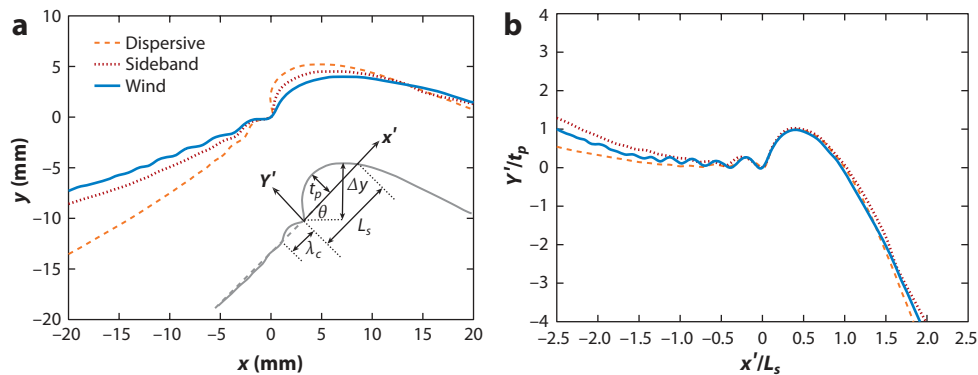
Figure 2

Crest profiles of spilling breakers generated by three different methods and their geometric similarity.
Figure adapted from Diorio et al. (2009).

results, spilling breakers are initiated by the formation of a bulge, the appearance of parasitic capillary waves, and the subsequent breakdown of the bulge into turbulence in the crest's forward face. In a subsequent study, Duncan et al. (1999) measured detailed crest-profile histories of spilling breakers. The evolution of the maximum surface elevation (as well as the length and the thickness of the bulge, the location of the toe, and the capillary waves) was measured to describe the crest shape deformation. The front faces of the crest profile prior to the bulge becoming turbulent are geometrically similar, independent of the wavelength of the spillers. This geometric similarity was investigated further and validated in a recent experimental study by Diorio et al. (2009), who adopted three different methods (i.e., dispersive focusing, modulational instability, and wind forcing) to generate unsteady spilling breakers with lengths of 10 to 120 cm. With a high-speed imager and laser-induced fluorescence, they measured the crest profiles close to breaking and found that, when scaled appropriately, the bulge and capillary waves on the crest-front faces of the spillers (at breaking onset) are self-similar, independent of the breaking-wave-generation mechanism (**Figure 2**). Note that the geometric similarity is limited to the crest-front profiles of the spillers. This similarity was attributed to the crest flow being dominated by surface tension and gravity (Duncan 2001, Diorio et al. 2009).

The crest shape deformation of plunging breakers is also of interest. Bonmarin (1989, figure 6) observed wavelength reduction and wave-crest growth as the crest evolved to a plunger. The depth of the trough in front of the breaking crest initially increased and achieved a maximum at approximately one to two wave periods before breaking onset. At this stage, the crest elevation is roughly equal to that of the trough, and no evident horizontal asymmetry occurs. As the wave further evolved and the crest continued growing, the surface elevation at the trough became shallower and even rose above the mean water level. The crest-front steepness increased more than twofold during the process. Tian et al. (2012) examined the crest growth and wavelength reduction of breaking waves due to both dispersive focusing and modulational instability. They found that spillers and plungers have approximately the same wavelength-reduction rate, i.e., approximately a 30% reduction of the wavelength within two wave periods before breaking onset. Meanwhile, the crest height of spillers may increase as much as 20% within one wave period before breaking onset, whereas plunging crests may become twice as large during the same period. Diorio et al. (2009) observed that the crest height of spillers may grow 15% within one-fourth of a wave period prior to breaking onset. According to these observations, it may be argued that wavelength

decrease is the dominant factor in the steepening of a crest that subsequently develops into a spiller; however, both wavelength reduction and wave-crest growth are significant in the generation of plungers.

One characteristic of plunging breakers is the overturning crest due to a projected water jet from the wave-crest front. Longuet-Higgins (1981, 1982) parameterized the forward face of an overturning plunger at initial stages with cubic curves. New (1983) showed that part of the surface profiles underneath the overturning crest may be represented with an ellipse of axes ratio $\sqrt{3}$. This ellipse model was validated qualitatively in the experimental study of Bonmarin (1989). Many subsequent experimental studies also examined the overturning crests of plungers (e.g., Perlin et al. 1996, Skyner 1996, Chang & Liu 1998, Melville et al. 2002, Drazen et al. 2008), although most of the studies focused on the kinematics and dynamics rather than the geometry of the breaking crests. Interestingly, Drazen et al. (2008) defined and determined a falling crest height, h, in their inertial scaling of energy dissipation of unsteady breaking waves. The falling crest height is the vertical distance from the maximum surface elevation to the point at which the overturning crest just impacts the water surface beneath it. Their theoretical analysis showed that the energy dissipation rate due to plunging breakers may be parameterized with the falling crest height, i.e., $D \sim (kh)^{2/5}$. Here D is the energy dissipation rate due to breaking. Tian et al. (2012) further examined the falling crest height in their development of an eddy viscosity model for breaking waves. They found an approximately linear relationship between the falling crest height and a crest asymmetry parameter, i.e., $kh \sim R_b$. Here $R_b = \beta/(1 + \beta)$, and β is the vertical asymmetry parameter of the breaking crest.

In conclusion, many prior studies had focused on the straightforward quantification of wave geometric properties such as the limiting steepness, breaking crest asymmetry, and the evolution of breaking crest profiles in an attempt to understand the fundamental physics of breaking waves. Recent progress in the study of the geometric properties of breaking waves has evolved to the point at which we can identify possible connections between the breaking crest geometry and the breaking-wave dynamics, i.e., energy dissipation and dissipation rate (e.g., Drazen et al. 2008; Tian et al. 2010, 2012). Additional work on this topic that considers the influence of three-dimensionality, wind forcing, and currents, for example, may lead to more significant contributions in the future.

3. WAVE-BREAKING-ONSET PREDICTION

The accurate prediction of wave-breaking onset is challenging and has been the focus of many investigations. Numerous breaking criteria have been proposed through theoretical analysis, numerical simulations, laboratory experiments, and field observations (Nepf et al. 1998, Wu & Nepf 2002, Oh et al. 2005, Tian et al. 2008). Based on the predicting parameters involved, they can be classified into three categories, i.e., geometric, kinematic, and dynamic breaking criteria.

3.1. Geometric Breaking Criteria

In the following, criteria for 2D breaking are discussed first. Subsequently a brief discussion follows on the 3D effects of breaking criteria as well as the effects of wind and currents.

3.1.1. Geometric criteria for two-dimensional incipient breaking. Geometric criteria typically use the limiting steepness associated with incipient wave breaking as a critical parameter to predict breaking onset. As discussed in Section 2.1, the limiting steepness measured in laboratory experiments ranges from 0.15 to 0.44. This variation renders improbable the universal application of limiting steepness for breaking-onset prediction. However, Babanin et al. (2007, 2010) recently

conducted numerical simulations and experimental measurements of breaking waves due to modulational instability, arguing that it is the limiting steepness $ka \sim 0.44$ that ultimately triggers wave breaking. They introduced an initial monochromatic steepness (IMS) to predict breaking onset. It was shown that waves of IMS > 0.44 break immediately (within one wavelength) and waves of IMS < 0.08 will never break in the absence of wind forcing. Waves with IMS between the two limits will evolve eventually to breaking, and that distance decreases with increasing IMS. The finding is interesting, but the determination of the IMS is problematic as it does not exist for evolving wave groups in the ocean or, for that matter, even in the laboratory. Note that for modulated wave groups that eventually lead to breaking, the reported initial carrier wave steepness ka is approximately 0.11 (e.g., Tulin & Waseda 1999, Chiang & Hwung 2007).

Alternatively, Rapp & Melville (1990) proposed a global steepness, $S = k_c(\Sigma a_n)$, associated with wave groups to predict breaking onset due to dispersive focusing. A critical global steepness $S_0 = 0.25$ worked well in their study. Here k_c is the wave number of the center frequency wave in the wave group, and a_n is the amplitude of the n-th wave component. Later, it was shown that the critical global steepness can be affected by the wave spectral shape; e.g., Chaplin (1996) reported $S_0 = 0.265$ and 0.30 for wave groups of constant-amplitude and constant-steepness spectra, respectively. Banner & Peirson (2007) found that the critical global steepness associated with breaking waves due to modulational instability can be as low as 0.12. Drazen et al. (2008) defined the global steepness as $S = \Sigma(k_n a_n)$ and reported that breaking onset due to dispersive focusing is in the range 0.32–0.36. Here k_n is the wave number of the n-th wave component. Tian et al. (2010) proposed an alternative definition of the global steepness by replacing k_c with a spectrally weighted wave number k_s, i.e., $S = k_s(\Sigma a_n)$, for wave groups of constant-steepness spectra and identified a critical value of 0.34 for breaking onset.

The crest's geometric parameters, especially the crest-front steepness, are more suitable for describing the local crest geometry and are often considered more robust than ka for breaking-onset prediction. For 2D breaking waves, the reported critical crest-front steepness is 0.32 in Kjeldsen & Myrhaug (1979) and Kjeldsen et al. (1981); 0.31 in Bonmarin (1989); from approximately 0.31 to 0.34, depending on frequency bandwidth, in Rapp & Melville (1990); and 0.38 in Wu & Nepf (2002). These critical values are not necessarily associated with incipient wave breaking, which is not well documented in the studies. Also concentrating on the crest's geometric parameters, Babanin et al. (2007, 2010) measured the asymmetry (A_s) and the skewness (S_k) of incipient breakers due to modulational instability. They reported that the former varies from approximately -0.33 to 0.75 and the latter from 0 to 1 (Babanin et al. 2010, figure 10), corresponding to a vertical asymmetry $\beta = 0.57 \sim 1.49$ and horizontal asymmetry $\mu = 0.5 \sim 0.67$, respectively.

Overall, the forecasting parameters used in geometric criteria are simple and relatively straightforward to determine, which may explain why they have been the focus of so many studies. Unfortunately, the use of simple geometric parameters has compromised the universality of this type of criterion. Wave breaking can be generated through different mechanisms, such as dispersive focusing, modulational instability, wind forcing, and wave-current interaction. The generation mechanism can influence breaking-wave geometry at the onset, as discussed in the next section. In addition, wave breaking occurs over a wide range of length scales, and waves of the same length scale may break with different intensity, which means that predicting breaking onset from only geometric aspects was destined to fail. Furthermore, the wave profile close to breaking has an irregular shape and evolves rapidly in time and space, which may complicate the definition and determination of incipient wave breaking.

3.1.2. Three-dimensionality, wind, and current effects. This section discusses the effects of three-dimensionality, wind, and current on wave-breaking onset in terms of their influence on

geometric breaking criteria. We begin with the 3D wave experiments conducted by Johannessen & Swan (2001), who showed that the increase in directional spread (i.e., more short-crested waves) effectively reduces the maximum crest elevation, η_{max}, at the focusing point for the same overall wave stroke of their wave maker. Therefore, to generate limiting 3D waves (incipient breakers) with greater directional spread, they used a larger overall stroke input, which resulted in a higher crest elevation of the limiting waves. The wave steepness represented by $k_p \eta_{max}$ of the 3D limiting waves can be as much as 35% greater than that of 2D limiting waves. Here k_p is the spectral peak wave number. However, one should notice that the steepness is calculated with k_p rather than a local wave number. Consistent with Johannessen & Swan, Waseda et al. (2009) observed that the occurrence of freak waves in their random directional wave field rapidly decreased as the directional spread increased.

Toffoli et al. (2010) recently reported that the limiting steepness of 3D ocean waves can reach a maximal steepness of 0.55 (much higher than the Stokes breaking limit), beyond which the waves will break. However, it was documented that waves of this maximal steepness are already breaking. By comparing field and laboratory measurements, Toffoli et al. argued that the maximal steepness is a property of the waves rather than a feature of the evolution or environmental conditions. Babanin et al. (2011) made additional contributions to the estimation of the limiting steepness of 3D waves. Their results show that the limiting steepness associated with the onset of wave breaking is $ka = 0.46$–0.48, whereas the steepness may reach $ka \sim 0.55$ during the course of breaking. The associated limiting horizontal asymmetry μ is approximately 0.63, slightly less than 0.67 as reported in their previous study of 2D incipient breakers (Babanin et al. 2010).

Wind forcing is also known to affect the limiting steepness of incipient breaking waves. Banner & Phillips (1974) showed theoretically that the presence of a wind-driven surface drift can substantially reduce the maximum surface elevation, $\zeta_{max} = C^2(1 - q/C)^2/(2g)$. Here C is the wave phase speed, and q is the magnitude of the surface drift. Therefore, the limiting steepness for incipient wave breaking is $ka = (1 - q/C)^2/2$. Reul et al. (1999) observed the airflow structure above steep and breaking waves using particle image velocimetry (PIV). Although their study was not designed to examine geometric breaking criteria, their measurements showed that the crest-front-face steepness at incipient breaking ranges from ~0.15 to 0.30, much less than that of incipient breaking in the absence of wind (typically greater than 0.30) (Reul et al. 1999, figure 2). Touboul et al. (2006) and Kharif et al. (2008) examined the evolution of dispersive focusing wave groups under wind forcing, which was found to sustain the duration of extreme waves and delay the defocusing process of the focusing groups. They identified a critical local surface slope $\partial \eta / \partial x = 0.35$ to indicate the onset of airflow separation, which is generally accompanied by wave breaking. As limiting Stokes waves have a mean slope of $\tan(\pi/6) = 0.58$, wave breaking under wind forcing may occur at a much reduced surface slope. Recently, Babanin et al. (2010) examined the evolution of modulated wave groups under wind forcing. They showed that wind influences incipient breaking by stabilizing the crest shape before breaking onset (reducing the scattering of the limiting geometric parameters) but then randomizing the crest shape of breaking waves. However, they argued that the overall wind-forcing effect on breaking onset is generally minimal unless very strong wind is present.

As for the effects of current on geometric breaking criteria, the studies by Wu & Yao (2004) and Yao & Wu (2005, 2006) are particularly interesting. Wu & Yao (2004) reported that weak uniform (either following or opposing) currents have limited influence on incipient wave breaking. However, strong opposing currents can increase significantly the limiting steepness (to 0.36), which also depends on the shape and bandwidth of the wave frequency spectra. Furthermore, Yao & Wu (2005, 2006) observed that the limiting steepness of incipient breaking waves depends strongly on shear currents; i.e., positive (negative) shear currents decrease (increase) the limiting

steepness, and the variation of the limiting steepness is proportional to the shear strength of the current. Specifically, the limiting steepness of their incipient breakers decreases from 0.18 to 0.16 as the current shear strength varies from −0.5 to 0.8.

3.2. Kinematic Breaking Criteria

Kinematic breaking criteria often involve the horizontal crest particle velocity U and the wave phase speed C, and wave breaking occurs when U exceeds C; i.e., $U/C \geq 1$. The examination or application of this criterion is nontrivial because of the difficulties in determining U and the ambiguity in defining C of highly unsteady, rapidly evolving breaking crests. Nevertheless, kinematic criteria have drawn much attention.

The examination of kinematic criteria is facilitated by PIV measurements of breaking waves. Perlin et al. (1996) conducted PIV measurements of a deep-water plunging breaker created by dispersive focusing. They found that the measured phase speed C was close to its linear theory approximation, i.e., 1.08 versus 1.05 m s^{-1}. Just prior to the wave crest overturning, the maximum U was 0.8 m s^{-1}, which gave $U/C = 0.74$. However, when the crest front neared vertical, the water-particle velocities became virtually horizontal and began to accelerate. It was found that U at the tip of the ejecting jet of the plunging breaker was 30% greater than C. Chang & Liu (1998) performed PIV measurements of a monochromatic breaking wave in shallow water. They reported $U/C = 0.86$ prior to wave breaking and $U/C = 1.07$ when the particle velocities at the crest tip became almost horizontal. In addition, the velocity at the tip of the overturning jet was 68% greater than the linear wave phase speed. Both studies support kinematic breaking criteria.

Qiao & Duncan (2001) observed the evolution of the crest flow of gentle spilling breakers using PIV measurements. According to their measurements, the maximum horizontal particle speed U is approximately 75% to 95% of the breaking crest speed, C_b, before the toe moves; however, U/C_b increases to 1.0 to 1.3 following the initial motion of the toe (in wave coordinates). Recent estimations show that C_b is approximately 80% to 90% of the breaking-wave phase speed C (Melville & Matusov 2002, Banner & Peirson 2007, Tian et al. 2010). Stansell & MacFarlane (2002) examined kinematic criteria by conducting PIV measurements and by assessing three definitions of the wave phase speed (i.e., phase speed based on linear wave theory, partial Hilbert transforms of measured surface elevation, and the local position of maximum surface elevation). The estimated phase speed based on the three definitions showed great disparity. But all estimates were greater than the measured U, specifically, $U/C \leq 0.95$ for spilling breakers and $U/C \leq 0.81$ for plunging breakers. This suggests that $U/C \geq 1$ may be only a sufficient but not necessary condition for the onset of wave breaking. Using a PIV system, Oh et al. (2005) also evaluated kinematic breaking criteria for deep-water waves under strong wind forcing. The maximum U/C observed in their experiments was approximately 0.75, which led them to the conclusion that this kinematic criterion is inadequate for the prediction of breaking onset under wind action.

Conversely, Wu & Nepf (2002) examined kinematic criteria with surface-elevation measurements at fixed locations. C and U were estimated with the Hilbert transform and linear wave theory. It was reported that $U/C \geq 1$ successfully distinguished breaking waves from nonbreaking ones. Interestingly, the magnitude of U/C indicated variation of breaking strength along a single 3D breaking crest; i.e., $U/C \geq 1.5$ for plungers and $U/C \geq 1$ for spillers. They argued that this kinematic criterion is robust and insensitive to wave directionality. Considering that the results are based entirely on wave-probe measurements and linear wave theory, further evaluation may be necessary.

3.3. Dynamic Breaking Criteria

While downward acceleration at the wave crest and energy variation of higher-frequency wave components are often considered in the determination of dynamic breaking criteria, here we focus on dynamic criteria based on the local energy growth rate (Schultz et al. 1994, Banner & Tian 1998, Song & Banner 2002). Rapp & Melville (1990) hinted that the rate of change of wave steepness may perform better than the steepness itself for breaking-onset prediction. Schultz et al. (1994) reported one of the earliest numerical studies on this type of breaking criterion and demonstrated that a root-mean-square wave height [square root of potential energy, $\sqrt{\int \zeta^2(x) dx}$] can function as a breaking criterion for regular 2D deep-water waves. The critical condition is that the potential energy exceeds 52% of the total energy of a limiting Stokes wave. The authors also found that the energy input/growth rate can indicate the breaking severity. Later, Banner & Tian (1998) examined numerically the evolution of the local mean energy and momentum densities of waves subject to modulational instability. Two dimensionless growth rates, β_E and β_M, were constructed as the predicting parameters for breaking onset, and the threshold was determined as $\beta_{E/M} = 0.2$, independent of wave-group structures, initial wave-group configurations, and surface shears.

Their dynamic criterion was developed further in the numerical study of Song & Banner (2002), who proposed a dimensionless diagnostic parameter, $\delta(t)$, to represent essentially the growth rate of the mean local wave energy. The diagnostic parameter is a function of the local wave number and the local energy density at the envelope maxima of wave groups. With a threshold range for $\delta(t)$ of $(1.4 \pm 0.1) \times 10^{-3}$, the criterion was shown to successfully differentiate breaking waves from nonbreaking ones. The initial wave-group structure (as well as the number of waves in the wave groups, wind forcing, and surface shear) has little influence on the threshold range (Banner & Song 2002), which indicates the universality of the criterion for breaking-onset prediction. Moreover, a strong correlation was presented between the breaking parameter, $\delta(t)$, just prior to breaking onset and the breaking intensity indicated by the global steepness, as proposed by Rapp & Melville (1990). Note that Song & Banner (2002) generated breaking waves through both modulational instability and dispersive focusing.

The evaluation and validation of dynamic criteria were the focus of several experimental efforts (Banner & Peirson 2007; Tian et al. 2008, 2010). Banner & Peirson (2007) conducted detailed laboratory experiments in which they generated and examined wave groups with the same or equivalent initial conditions as in Song & Banner's numerical simulations. The local wave-energy density and the local wave number at the wave-group envelope maxima were determined through surface-elevation measurements using two sets of three in-line wave probes. Experimental results were supportive of the dynamic criterion published by Song & Banner (2002). Concurrently, Tian et al. (2008) performed independent laboratory experiments to evaluate the breaking criterion. Unlike the experimental reproduction of Song & Banner's initial conditions in Banner & Peirson (2007), Tian et al. generated breaking waves through dispersive focusing and measured the surface profile as a function of time and space using video imaging. With the measurements and complementary numerical simulations, they found that the criterion is sensitive to the choice of local wave number, but the adoption of a particular local wave number determined by two consecutive zero crossings adjacent to the breaking crest allows the criterion to distinguish breaking groups from those that do not break. Further validation was provided by Tian et al. (2010), who investigated four additional dispersive focusing groups with different characteristic frequencies. In addition, the diagnostic parameter just prior to wave breaking was found to correlate well with the breaking strength parameter suggested by Duncan (1981, 1983).

Dynamic criteria based on the local wave-energy growth rate appear robust; however, their application in phase-resolving, deterministic prediction of the evolution of nonlinear wave fields

may be limited, as the calculation of the diagnostic parameter $\delta(t)$ is nontrivial. The process involves the estimation of the dimensionless local energy oscillating at the maximum surface elevation, the determination of its upper and lower envelopes using spline fitting, and the computation of the mean local energy growth rate.

4. ENERGY DISSIPATION IN BREAKING WAVES

4.1. Estimation and Parameterization of the Total Dissipation

Wave breaking dissipates energy through the entrainment of air bubbles into the flow and the generation of currents and turbulence (Rapp & Melville 1990, Lamarre & Melville 1991). Over the course of many years, laboratory experiments have been conducted extensively for the estimation and parameterization of the total energy dissipation (e.g., Rapp & Melville 1990; Banner & Peirson 2007; Drazen et al. 2008; Drazen & Melville 2009; Tian et al. 2008, 2010). Ideally the estimation requires direct measurement of the surface profile and the velocity field over a fairly large field of view throughout the active breaking process, which proves extremely difficult in both field and laboratory experiments (Melville et al. 2002, Drazen & Melville 2009). Alternatively, it may be approximated through surface-elevation measurements at fixed locations upstream and downstream of wave breaking and through implementation of a wave theory and a simple control volume analysis. A demonstration of the control volume analysis can be found, e.g., in Rapp & Melville (1990, section 2.4 and figure 5).

One of the first experimental studies that systematically quantified and parameterized energy dissipation due to wave breaking was performed by Rapp & Melville (1990), who reported that a spilling breaker can dissipate as much as 10% of the initial energy of a dispersive focusing group, whereas more than 25% can be dissipated during a plunging breaking event. The energy dissipation was inferred with surface-elevation measurements and control volume analysis under the assumptions of linear wave theory, i.e., $\Delta E/E_0 = \Delta[\zeta^2]/[\zeta(x_0, t)^2]$. Here ΔE is the energy dissipation, E_0 is the total prebreaking energy at a reference location x_0, $\Delta[\zeta^2] = [\zeta(x_1, t)^2] - [\zeta(x_2, t)^2]$ with $\zeta(x,t)$ the temporal surface elevation measured at the x locations, and the square brackets represent long time integrations. The authors found that $\Delta E/E_0$ depends strongly on the global wave steepness S (**Figure 3a**). The influence of wave-group bandwidth and carrier frequency on the energy dissipation was shown to be weak and secondary. Using the same technique, subsequent studies quantified the energy dissipation of wave breaking due to dispersive focusing considering different initial wave spectral shapes (Kway et al. 1998), free wave dissipation by excluding contributions from bound waves (Meza et al. 2000), three-dimensionality (Nepf et al. 1998, Wu & Nepf 2002), and currents (Yao & Wu 2004).

Banner & Peirson (2007) estimated and parameterized the energy dissipation in breaking waves using the diagnostic parameter $\delta(t)$ in the dynamic breaking criterion proposed by Song & Banner (2002). Song & Banner showed that the parameter just prior to wave breaking, δ_{br}, correlates well with the energy dissipation due to wave breaking. Banner & Peirson managed to determine experimentally the energy dissipation (ΔE) and the prebreaking energy (E_0) for breaking waves produced with the same initial conditions as the numerical tests of Song & Banner. The focus of Banner & Peirson (2007) was to evaluate experimentally the dynamic breaking criterion; a majority of their breaking waves resulted from modulational instability, with the breaking intensity relatively mild. However, the mean dissipation averaged over the wave group can still be as large as 20% depending on breaking strength, and it has an approximately linear dependence on δ_{br} (**Figure 3b**).

Recently, Tian et al. (2010) reported interesting experimental results of the energy dissipation of plunging breakers due to dispersive focusing. They defined and determined three sets of
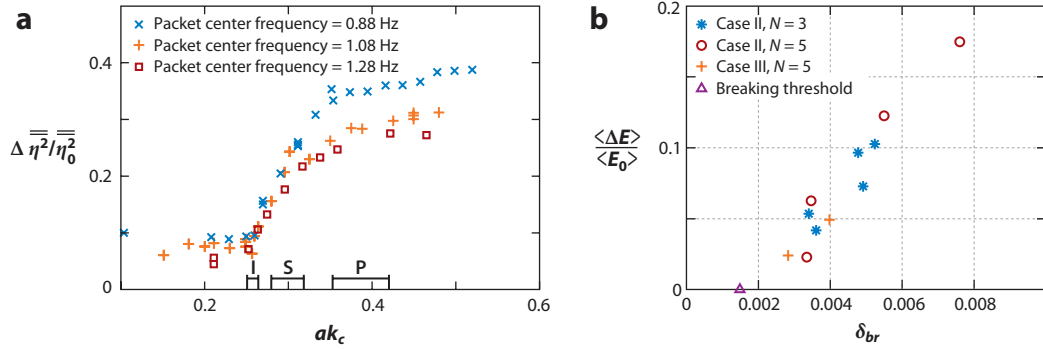
Figure 3

Parameterization of energy dissipation (*a*) as a function of global wave steepness *S* and (*b*) as a function of δ_{br}. In panel *a*, I, S, and P represent the range of steepness for incipient breaking, spilling breakers, and plunging breakers, respectively. Panel *a* redrawn from Rapp & Melville (1990), and panel *b* redrawn from Banner & Peirson (2007).

characteristic timescales and length scales (i.e., global scales associated with the wave group, local prebreaking scales prior to breaking onset, and local postbreaking scales of the subsequent breaking crest). They successfully demonstrated relationships among these sets, which were employed to parameterize the energy dissipation $\Delta E/E_0$. The energy dissipation ratio ranged from 8% to ~25% for their plungers. Both $E_0 k_s^3/(\rho g)$ and $\Delta E k_s^3/(\rho g)$ can be scaled accurately with the global steepness *S*, which indicates that $\Delta E/E_0$ is correlated well with *S*. Here k_s is a spectrally weighted wave number of the wave group.

4.2. Spectral Distribution of the Energy Dissipation in Breaking Waves

In laboratory experiments, frequency spectra evolution of breaking groups due to dispersive focusing has been examined frequently (e.g., Rapp & Melville 1990, Baldoc et al. 1996, Kway et al. 1998, Meza et al. 2000, Yao & Wu 2004, Tian et al. 2011). These studies show that as wave groups approach breaking, energy levels of the wave components of frequencies higher than the spectral peak grow at the expense of spectral peak reduction. Prior to breaking, similar energy upshifting can also occur for breaking-wave groups due to modulation instability (e.g., Babanin et al. 2010). In the subsequent breaking process, according to Tian et al. (2011), the energy gain across the higher-frequency region is dissipated. Direct comparison of the wave frequency spectra before and after breaking reveals that most of the energy dissipation is located at the high end of the first harmonic band ($f/f_p = 1$–2; here f_p is the spectral peak frequency) (**Figure 4**). In addition, the wave components of frequencies lower than the spectral peak propagate through the breaking event without much energy loss. If viscous dissipation is excluded, the spectral peak remains virtually unchanged (Meza et al. 2000, Tian et al. 2011). Conversely, for wave groups subject to modulational instability, wave breaking can significantly reduce the spectral peak, and a spectral peak downshift can be observed after breaking (e.g., Tulin & Waseda 1999, Hwung et al. 2007).

Meza et al. (2000) generated isolated spillers and plungers with dispersive focusing and managed to quantify the spectral distribution of energy dissipation due only to free waves by excluding the contributions from the bound waves. They reported that a small portion (~12%) of the breaking dissipation in the higher-frequency region is transferred to wave components of frequencies lower than the spectral peak. Yao & Wu (2004) investigated the energy dissipation in breaking waves subjected to currents. For breaking waves in the presence of strong opposing currents, their results showed that a larger portion (to 40%) of the dissipated energy in the
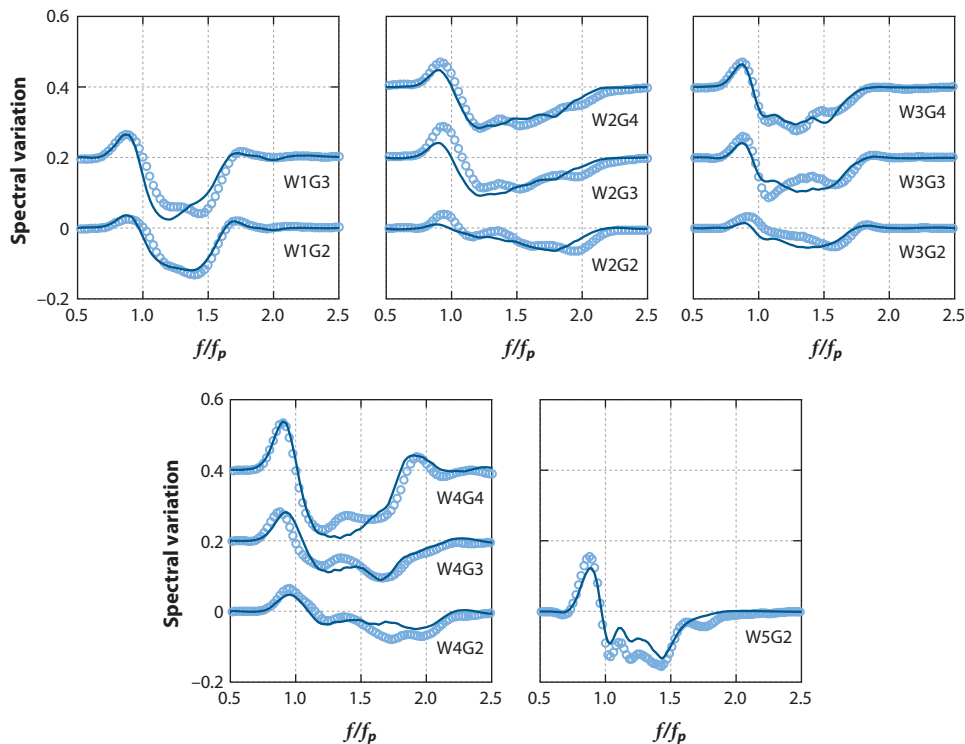
Figure 4

Variation in wave frequency spectra breaking-wave groups. W1G3 represents the first experimental wave train (W1) with the third gain setting (G3), for example. The solid curves are from numerical simulations, and the measurements are represented by open circles. Figure adapted from Tian et al. (2011).

higher-frequency wave components was transferred to the lower-frequency waves. Alternatively, Tian et al. (2011) suggested that the lower-frequency wave components may not necessarily gain energy directly from the higher-frequency waves. By tracking the energy level in the lower frequencies ($f/f_p = 0.5$–0.9), they found that energy gain in the region occurred before breaking onset, and for more than half of the breaking groups considered, no obvious energy gain was found immediately following wave breaking. Therefore, Tian et al. argued that this energy gain (see **Figure 4**) may result from the combined effects of nonlinearity and wave breaking. They determined that energy is transferred to the lower-frequency region through nonlinearity (from the spectral peak) in the focusing process and that the presence of wave breaking rendered irreversible the nonlinear energy transfer (back to the spectral peak) during the defocusing process. Note that the nonlinear transfer is reversible in the absence of wave breaking (Tian et al. 2011).

4.3. Energy Dissipation Rate During Active Wave Breaking

In this subsection the timescale of dissipation is necessarily discussed first. This is followed by a discussion of energy dissipation and its parameterization.

4.3.1. Timescale of energy dissipation in breaking waves. Before proceeding to the estimation of the energy dissipation rate in wave breaking, a discussion of the relevant timescales is
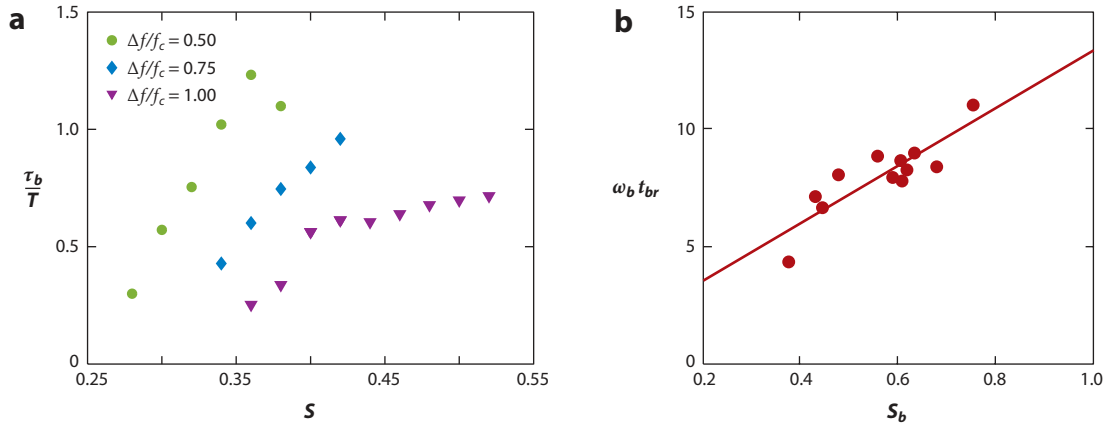
Figure 5

Active breaking duration as a function of global wave steepness (breaking strength). Panel *a* adapted from Drazen et al. (2008), and panel *b* adapted from Tian et al. (2010).

appropriate. The duration of active wave breaking is of the order of one wave period (Rapp & Melville 1990, Lowen & Melville 1991, Dean & Stokes 1999, Drazen et al. 2008, Tian et al. 2010), and most of the energy dissipation occurs during the active breaking process. Lamarre & Melville (1991) demonstrated that entraining air into water, which accounts for 30% to 50% of the total energy dissipation, happens within a small fraction of a wave period. Rapp & Melville (1990) and Melville et al. (2002) showed that 90% of the total energy dissipation is completed within the first four wave periods following breaking onset, and the remainder decays as t^{-1}. Chen et al. (1999) performed numerical simulations of breaking waves and reported that 80% of the total energy is lost within three periods of breaking onset. Therefore, the notion of active breaking duration has been employed by several researchers in the estimation of the energy dissipation rate (Melville 1994, Drazen et al. 2008, Tian et al. 2010). Lowen & Melville (1991) measured the duration of the acoustic sound generated by wave breaking; Melville (1994) applied their measurements to deduce the associated energy dissipation rate. Similarly, Drazen et al. (2008) estimated the energy dissipation rate via active breaking duration as inferred from hydrophone measurements of the acoustic signal. It was found that the active breaking time depends on the global wave steepness (and breaking strength) (**Figure 5a**). Alternatively, Tian et al. (2010, 2012) determined the active breaking timescales and length scales by observing whitecap coverage due to wave breaking. As shown in **Figure 5b**, the active breaking time also exhibits a strong dependence on breaking strength, although the breaking times are in general much greater than those measured by Drazen et al. (2008).

4.3.2. Parameterization of energy dissipation rate. The energy dissipation rate of 2D breaking waves scales to the fifth power of a characteristic speed; i.e., $\varepsilon = b\rho U^5/g$. Here ε is the dissipation rate per unit crest width, ρ is the water mass density, U is a characteristic speed associated with the breaking wave, and b is a dimensionless coefficient related to wave-breaking strength (termed the wave-breaking strength parameter). The estimation and parameterization of ε are important in phase-averaged wave modeling. The parameterization originated from the seminal experimental work by Duncan (1981, 1983). Moreover, because of its importance in relating the kinematics to the dynamics of breaking waves, the above equation has been investigated extensively in laboratory experiments and field observations (e.g., Duncan 1981, 1983; Phillips 1985; Thorpe 1993; Melville

1994; Phillips et al. 2001; Melville & Matusov 2002; Banner & Peirson 2007; Drazen et al. 2008; Drazen & Melville 2009; Gemmrich et al. 2008; Tian et al. 2010).

It would be beneficial if a particular choice of the characteristic speed U associated with the breaking wave can provide a universal, constant b; unfortunately, it is unlikely that such a choice of U exists as there can be a wide range of breaking intensities for a wave of given length. To date, the speed choices are the breaking crest speed, C_b, and the breaking-wave phase speed, C; the former has been adopted more frequently. Recently, Banner & Peirson (2007) employed the breaking-wave phase velocity in their estimation of the dissipation rate. This was done because ocean wave modeling is performed often in the frequency domain, and the wave phase speed C of the Fourier wave components is easier to determine than the breaking crest speed C_b. Note that laboratory and field measurements have shown that C_b can be approximated by a fraction of C, for example, $C_b/C = 0.8$ in Melville & Matusov (2002), 0.9 ± 0.04 in Banner & Peirson (2007), and 0.84 in Tian et al. (2010). Therefore, the use of one speed as opposed to another will result in a different, but correlated, breaking strength parameter b.

The estimation of the energy dissipation rate was reported first by Duncan (1981, 1983), who generated quasi-steady breaking waves by towing a submerged hydrofoil and measured the induced drag per unit crest width, F_b. The drag was found to scale with the fourth power of the breaking-wave phase speed; i.e., $F_b = 0.009\rho C_b^4/(g\sin\theta)$. Here θ is the angle of inclination of the breaking region. Therefore, the energy dissipation rate per unit crest width was determined as $\varepsilon = F_b/C_b = b\rho C_b^5/g$ (Duncan 1981, 1983; Phillips 1985; Thorpe 1993; Melville 1994). According to Duncan (1981), θ ranged from $10°$ to $14.7°$, which gives a breaking strength parameter $b = 0.009/\sin\theta = (3.6–5.2) \times 10^{-2}$.

Focusing on unsteady breaking waves, Melville (1994) determined the energy dissipation rate by examining the turbulence dissipation rate due to wave breaking. With the assumption that the lost energy due to breaking is eventually transferred to heat through viscosity, the energy dissipation rate per unit crest width is $\varepsilon = \rho u^3/l(DL/2)$. Here u and l are an integral velocity and length scale associated with the wave turbulence, respectively; D and L are the depth and length of the roughly triangular turbulent region, respectively (see Rapp & Melville 1990, section 4, and Melville 1994, section 5). According to Rapp & Melville's (1990) dye-patch experiment to determine the spatial extent of the turbulent mixing, $u \sim \chi C$, $l \sim D$, and L is comparable to the breaking wavelength; i.e., $L \sim 2\pi C^2/g$. Therefore, the dissipation rate can be estimated as $\varepsilon = (\pi\chi^3)\rho C^5/g$. The numerical constant χ is estimated as 0.10–0.17 (Melville 1994, Tian et al. 2010). Therefore, the breaking strength parameter $b = \pi\chi^3$ varies in the range $(3–16) \times 10^{-3}$. The estimation is somewhat lower than that of Duncan (1981, 1983), mainly because the type of breakers and the breaking intensity vary in the different studies.

Alternatively, b can be directly estimated by determining the total energy dissipation and the active breaking time; i.e., the energy dissipation rate is estimated as $\varepsilon = \Delta E/t_b$, and the breaking strength parameter is then evaluated as $b = \varepsilon g/\rho U^5$ (Melville 1994, Drazen et al. 2008, Tian et al. 2010). Here the total energy dissipation ΔE and the active breaking time t_b can be determined as discussed above. Using this estimation method, Melville (1994) reanalyzed the measurements of Lowen & Melville (1991) and found that the breaking parameter is in the range $(4–12) \times 10^{-3}$. Drazen et al. (2008) conducted an inertial scaling analysis of the dissipation rate in unsteady breaking waves and derived $b = (bk)^{5/2}$. Here k was chosen as the wave number corresponding to the center frequency in the study and b the falling wave-crest height, which measures the height of the overturning crest when the crest just impacts the water surface below. The authors conducted experiments of breaking waves due to dispersive focusing in deep water to evaluate their theoretical results. Drazen et al. (2008, figure 13) found that $b = (1–7) \times 10^{-2}$, and their theoretical relation, $b = (bk)^{5/2}$, was valid only in a general sense owing to data scatter. The data

Figure 6
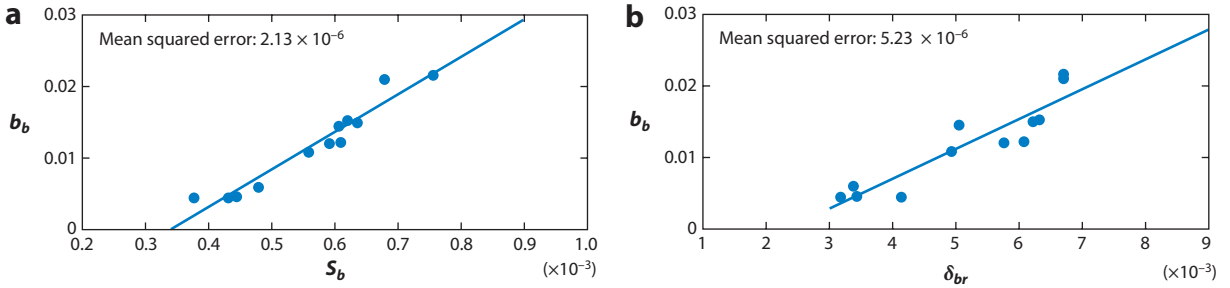
Normalized energy dissipation rate [breaking strength parameter (b_b)] as (*a*) a function of local wave steepness (S_b) and (*b*) the breaking criterion parameter δ_{br} by Song & Banner (2002). Figure adapted from Tian et al. (2010).

scatter may partially result from the utilization of the wave number of the center frequency wave, which is not necessarily a characteristic one. In both studies (Melville 1994, Drazen et al. 2008), t_b was measured with a hydrophone, and the characteristic speed U was chosen as the phase speed of the center frequency wave.

Tian et al. (2010) defined the characteristic wave-group velocity, local wave number, and breaking-wave phase speed. They used these quantities to estimate the breaking strength parameter (b_b in **Figure 6**), which was found to scale linearly with S (S_b in the figure) and δ_{br} and vary from 0.002 to 0.02. The estimate is in the same range given by Melville (1994) but is approximately one-third to one-half the value presented by Drazen et al. (2008) for comparable wave steepness. The discrepancy may be attributed to the different timescales adopted in the two studies. In addition, the application of the characteristic scales rather than the wave parameters corresponding to the center frequency in Tian et al. (2010) significantly reduced data scatter in their results.

Overall, the determination of the energy dissipation, as well as its spectral distribution and the dissipation rate due to wave breaking, has drawn much attention during the past two decades. Parameterization of the breaking-wave dissipation rate has benefited significantly from laboratory and field experiments, which have also advanced our understanding of the geometric properties and the kinematics of breaking waves. The combined effort has made available relationships among the three physics-based areas of breaking waves, i.e., links among the dynamics and the kinematics (e.g., $\varepsilon \sim \rho C^5/g$) and the parameterization of the dynamics using geometric properties [e.g., $b \sim S_b$ and $b \sim (hk)^{5/2}$].

5. PROGRESS REGARDING WAVE BREAKING AS MEASURED IN THE FIELD

Because of the difficulties and costs associated with field measurements of waves in deep and intermediate water depths, particularly breaking waves, as compared to laboratory and numerical investigations, progress has been slow; hence there are fewer studies to report. Obviously field measurements are inherently 3D, with breaking occurring sporadically and not necessarily near one's measurement location. Nevertheless, some hearty souls persevere, and we report their findings presently. Essentially all the existing results are related to dissipation due to wave breaking.

Thorpe (1993) used his own observations (Thorpe 1992) with wind speeds up to 28 m s^{-1} and a protected fetch of 20 km, along with those of several other researchers, to couple with the energy loss of a single breaking event in the laboratory (Duncan 1981) to estimate the energy transfer to the mixed ocean layer. He found that the number of breaking waves per wave is

$f = (4.0 \pm 2.0) \times 10^{-3} \times (W_{10}/c_0)^3$, where W_{10} is the wind speed at 10-m elevation and c_0 is the wave phase speed associated with the dominant waves. Then, using the energy loss per unit length of crest for a breaking wave, $E = (0.044 \pm 0.008)\rho c_b^5/g$, as found by Duncan, and knowing that $E_w = E f/\lambda_0$, he determined the energy loss per unit surface area due to breaking. Here c_b is the phase speed of the breaker; λ_0 is the wavelength of the dominant wave; and ρ and g are the mass density and acceleration of gravity, respectively. If a choice is made that c_b/c_0 is 0.25, as this ratio appears in the equation to the fifth power, then approximations are in order-of-magnitude agreement with the estimates of others. Thorpe made additional comparisons, for example, by looking at the dissipation values of Agrawal et al. (1992), and found agreement by simply changing the power of the phase speed ratio.

In a paper published for essentially the same purpose—for comparison with the field measurements by Agrawal et al. (1992)—Melville (1994) arrived at similar conclusions but used a different, perhaps more convincing, path. Melville argued compellingly that Duncan's (1981) measurements, which were achieved under quasi-steady breaking conditions using a submerged hydrofoil (e.g., as might be expected for ship-generated waves), might not be appropriate to represent ocean breaking waves that are likely unsteady. Melville estimated the energy dissipation rate per unit length of a crest based on data from Loewen & Melville (1991) and from Rapp & Melville (1990) and demonstrated order-of-magnitude agreement. Then, using this estimate, Melville stated that his phase speed ratio, c_b/c_0, had he needed one, would be ~0.40–0.63, as compared with that used by Thorpe (1993), 0.25 to match the Agrawal et al. data. Finally, it was shown that Melville's approximation is consistent with Phillips' (1985) field measurements. Additionally, we mention that improved data on the laboratory measurements are available presently but may not have been applied with regard to the field measurements.

Next we discuss attempts to determine the term in the wave action equation that remains most elusive: the dissipation (sink) term due to wave breaking (Komen et al. 1994). No definitive answer has evolved; however, much effort has been expended, and some progress has been made. The major difficulty in determining this term is that it requires field measurements of dissipation. Using data from a tower in Lake Ontario, Donelan (2001) assumed that an expression for the dissipation sink term is dependent on the saturation in the spectrum, with the degree of saturation $n = 2.5$ deemed the better choice. Because of long wave–short wave interaction, the equation must be modified, and comparisons across the entire spectrum are presented. The author acknowledged that more research is required to better quantify the constants in the equation.

Another parameter often used to obtain the dissipation term is $\Lambda(c)$. Using X-band radar, researchers from the Naval Research Laboratory conducted experiments that sensed the sea surface with high temporal and spatial resolution at Kauai, Hawaii, and these data were analyzed by Phillips et al. (2001) with regard to wave breaking. The average length of breaking front per unit area per unit speed, $\Lambda(c)$ as discussed originally in Phillips (1985), was given, $\Lambda(c) \approx \alpha c(\Sigma\tau^2)/(AT\Delta c)$, and using the data, the authors presented a first estimate. Here c is the phase speed, τ is the duration, α is a proportional constant that when multiplied by $c\tau$ yields the average length over the duration, A is the area of the sea surface considered, T is the observation time, and Δc is the difference in phase speed considered. **Figure 7** presents these seminal data. Additionally, the figure also presents the energy dissipated by wave breaking, as determined from their radar data, as a function of phase speed (through use of the expression in Duncan 1981).

Along similar lines, except by means of field data from aerial images recorded during the SHOWEX experiment, Melville & Matusov (2002) determined $\Lambda(c)$ and the energy dissipation due to breaking. They found that b in the Duncan (1981) expression was an order of magnitude larger than that found by Phillips et al. (2001) and suggested that this discrepancy might result from the indirect nature of the radar measurements. Using a weighting of U_{10}^{-3} (where U_{10} is of
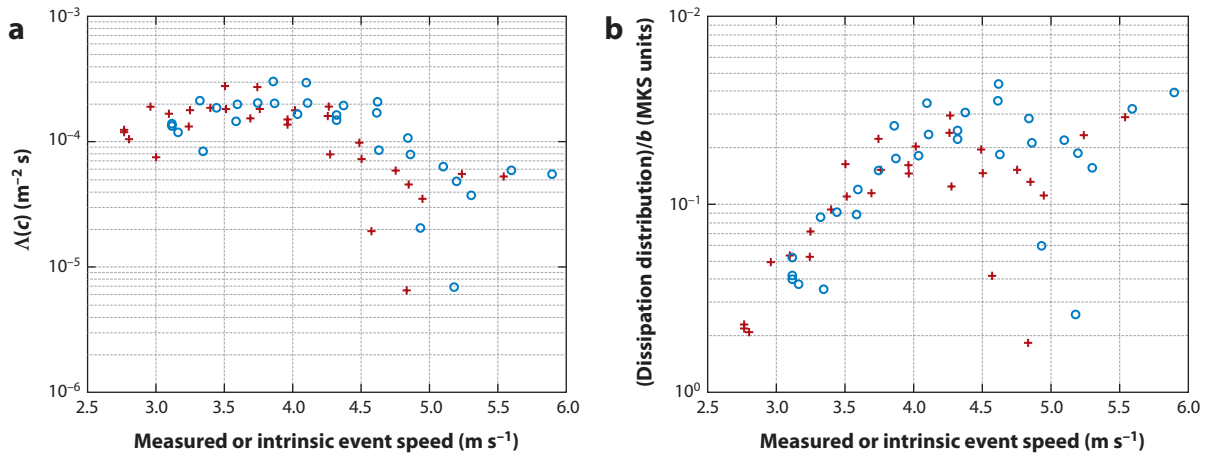
Figure 7

Determination of (*a*) Λ(*c*) and (*b*) the energy dissipation due to wave breaking as a function of speed. Figure redrawn from Phillips et al. (2001, figures 5 and 6), © American Meteorological Society. Reprinted with permission.

course the wind speed at 10 m), Melville & Matusov showed that the following expression fitted the data well: $\Lambda(c) = 3.3 \times 10^{-4} e^{-0.64c}$ over their measured range of speeds. For three distinct wind speeds and directions, they also presented the directional properties of $\Lambda(c)$, the momentum flux, and the energy dissipation.

Hwang & Wang (2004) also determined via field measurement a functional dependence for the dissipation term in the wave action density equation. They began with a form given by Phillips (1985) and sought to determine *B*, the so-called degree of saturation as a function of u_*/c, the ratio of the friction velocity to the wave phase speed. Their focus is on relatively short waves (0.02-m through 6-m wavelengths), and they necessarily divided their results into three regimes. For the lower wave numbers, the wave spectral function exhibits a power-law relation with exponent 1.0, whereas for the higher wave numbers, the exponent is 1.5. In their middle range of wavelengths (0.16 m through 2.1 m), the exponent of the degree of saturation, *B*, ranges to a maximum value of 10. They attributed this large change across the intermediate wave numbers to wave breaking but gave no further explanation.

Field measurements by Gemmrich et al. (2008) and subsequent analysis show agreement in some respects and disagreement in others with the papers discussed above. These researchers again determined $\Lambda(c) \, dc$ and found that over an intermediate range, $\Lambda(c)$ is larger, whereas at lower and higher scales, the value is significantly less. For developing seas, breaking waves were seen for a range of phase speeds about the spectral peak of 0.1 through 1.0. Conversely, for developed seas, breaking waves were rarely seen for phase speeds in excess of one-half the phase speed associated with the peak frequency. As in other papers, the authors computed the energy dissipation rate using the moments of $\Lambda(c)$. They also presented a value of *b* that is one to two orders of magnitude less than the results of Phillips et al. (2001) and Melville & Matusov (2002). Additionally, within their own data sets, *b* varies by a factor of three, and it increases with wave age. The authors suggested that for the open ocean, one should use a value of *b* as $(7 \pm 3) \times 10^{-5}$.

Once again alluding to the wave action density equation, Young & Babanin (2006) sought to determine the dissipation term. In citing preceding studies, the authors stated that none of the models addressed the physics of wave breaking. The authors followed the ideas of Zakharov and attempted to measure directly the spectral dissipation of wind-generated waves through "dominant"

breaking. Dominant breaking was defined as those breaking waves within the cyclic frequency range $f = f_p \pm 0.3f_p$, where f_p is the frequency associated with the peak of the spectrum. Breaking at smaller scales was considered a consequence of the dominant breaking waves. The data set used had almost a 50% rate of dominant breaking. The authors' primary conclusion was that the dominant breakers cause dissipation for the scales smaller than those of the spectral peak. The rate of dissipation at each frequency was found linear with the spectral density (less a threshold value) and a correction for the directional spectral width. Hence Young & Babanin found that the dissipation source term in the wave action density equation can be given by

$$S_{ds}(f) = agfX[F(f) - F_{thr}(f)] + bg \int_{f_p}^{f} [[F(q)] - F_{thr}(q)]A(q)\mathrm{d}q,$$

where a is a constant; g is the usual acceleration of gravity; F and F_{thr} represent the spectral density and a threshold spectral density, respectively; A is the directionally integrated form of the directional spectrum; and $X[\ldots]$ is to date an unknown function of its argument. As only a single data set was analyzed, the value of a determined was acknowledged to represent those particular conditions only. Furthermore and more importantly, the authors argued that their contribution was the first to estimate the spectral changes directly due to the breaking associated with the dominant waves.

With several ideas along the same lines as those of the two aforementioned papers, Banner & Morison (2010) proceeded to derive a model for the source terms in Komen et al.'s (1994) model under the assumption of negligible currents. For the right-hand side of the model, $S_{in} + S_{nl} + S_{ds}$ (which represents the total of the source terms due to the input from wind, the nonlinear wave-wave interactions, and the dissipation rate, respectively), the authors used contributions from Janssen (1991), which they modified, for what the authors called an "exact" form of S_{nl}, and, for the S_{ds} term, contributions from Banner et al. (2002) and Alves & Banner (2003) along with a new treatment that separated it into a local contribution and that of a background attenuation. For $\Lambda(c)$ and the (breaking strength) parameter, b, they used parts from Phillips (1985), Banner et al. (2002), and Banner & Peirson (2007) to obtain expressions for each for the value at the spectral peaks. In so doing, new forms for the wind input and source terms, as well as for $\Lambda(c)$ and b, were presented. **Figure 8** reproduces some primary results from this investigation, namely those for $\Lambda(c)$ and for S_{in}, S_{nl}, and S_{ds}.

As demonstrated above, many researchers have used the notions set forth by Phillips (1985) to quantify "the expected length of breaking fronts (per unit surface area) with speeds of advance between c and $c + \mathrm{d}c$ and the number of such breaking events passing a given point per unit time," i.e., $\Lambda(c)\mathrm{d}c$. Kleiss & Melville (2011) recently quantified these notions through the use of video recordings taken from aircraft. The authors went into great depth discussing the difficulties of quantifying regions of whitecaps from those that do not exhibit them, and the interested reader is referred to their paper. However, here we mention it as the results qualitatively support, for example, those mentioned previously by Melville & Matusov (2002) and Gemmrich et al. (2008).

On a slightly different track, similar to that in Section 2, Toffoli et al. (2010) used four large sets containing time series of independent data of sea surface elevation, two from field observations in the Black Sea and the Indian Ocean and two from directional wave basins, one in Norway and the other in Japan, to quantify wave steepness at breaking. Hence all records were from 2D surfaces. The authors divided the waves using zero upcrossings to obtain the rear wave statistics and zero downcrossings to define the statistics of the front portion of the wave. They found that the vertical extent of the waves changes little with breaking; rather the downcrossing period is reduced. Furthermore, their primary findings were that the front-face steepness is limited by 0.55,
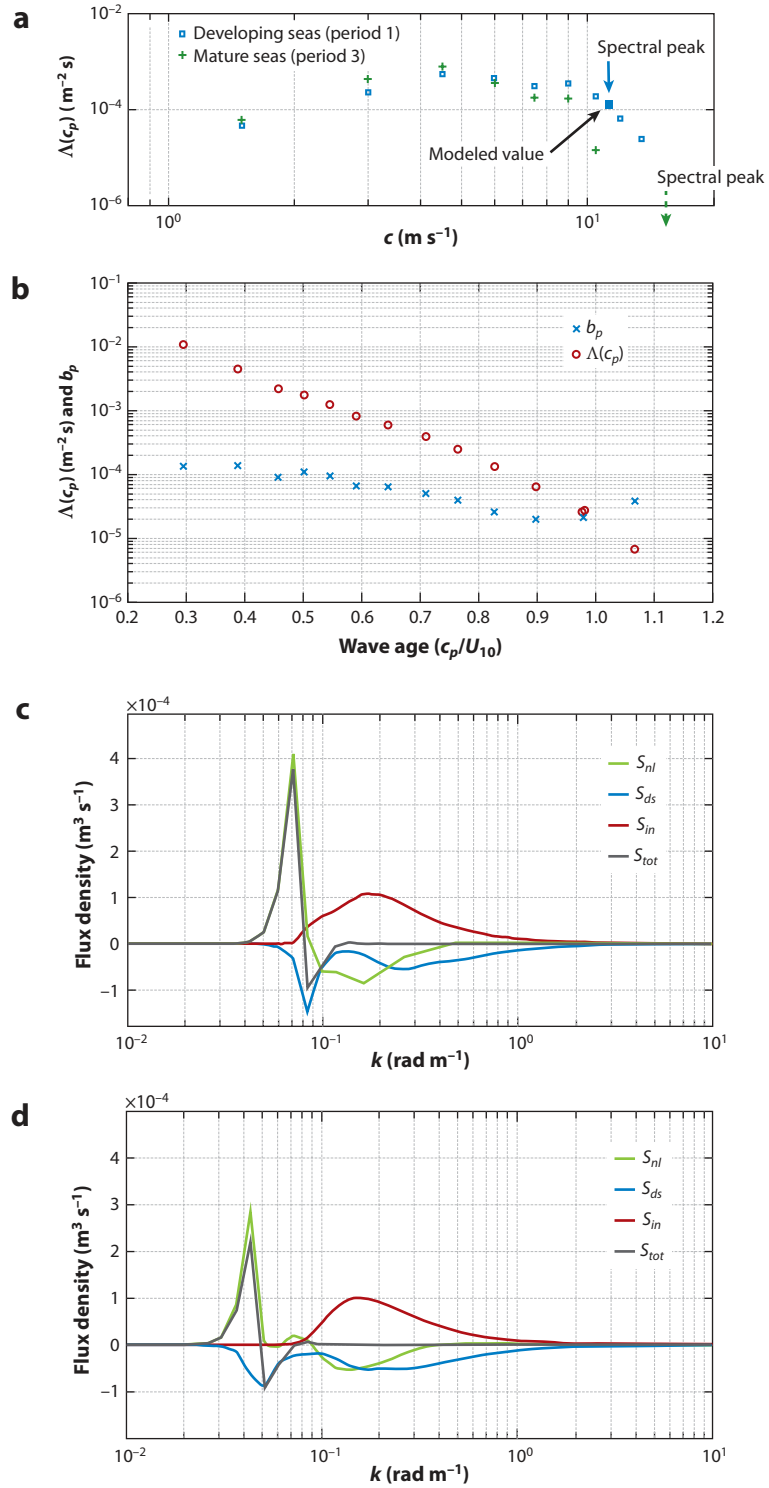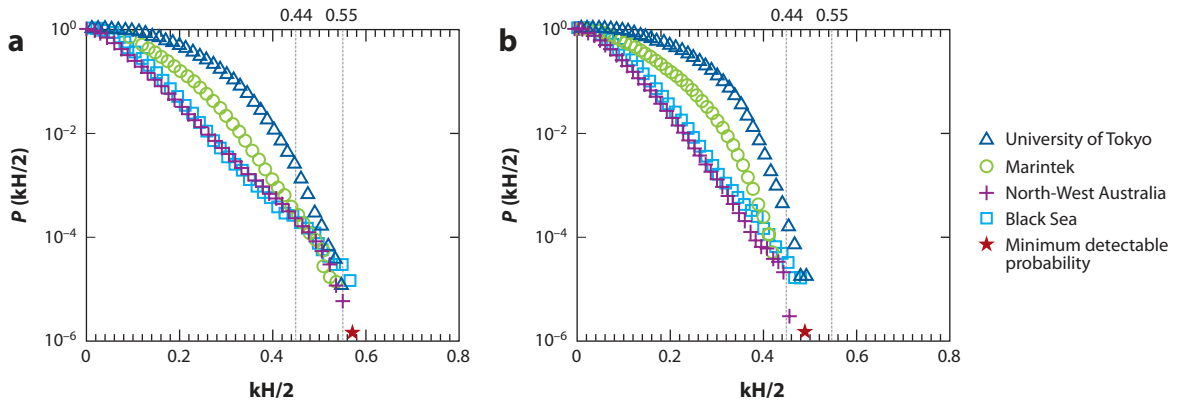
Figure 9

The wave steepness distributions for (*a*) downcrossing (front-face) waves and (*b*) upcrossing (rear-face) waves. As is evident, the front-face steepness is limited by 0.55, and the rear by slightly more than that of the Stokes wave, 0.44. A total of 5×10^5 observations were used in the study. Figure redrawn from Toffoli et al. (2010) by permission of the American Geophysical Union.

whereas the rear-face steepness exceeds the Stokes limiting value of 0.44 slightly. **Figure 9** exhibits nicely their principal conclusions.

It is clear from the discussions in this section that work on breaking waves in the field continues but that much remains to be done. Advances have been made in various areas; however, consensus among researchers is limited. The sluggish rate at which progress is being made is a result of the difficult nature of measurements in the field, as well as the costs associated with conducting these experiments.

6. NUMERICAL MODELING OF WAVE BREAKING

6.1. Inviscid Computations of Breaking Waves

The most well-known numerical method to compute breaking waves is the mixed-Eulerian-Lagrangian (MEL) method based on a boundary integral formulation. Following the seminal work of Longuet-Higgins & Cokelet (1976) for 2D breaking waves, a number of improvements have been made, including higher-order discretizations of the boundary geometry, fast algorithms to evaluate multiple integrals, and extensions to 3D waves possibly interacting with bottom to-pography with application to shallow-water waves. As there have been a number of extensive reviews on this method, including Tsai & Yue (1996), we do not provide a detailed description of numerical implementations here. Because the MEL method can simulate a breaking wave only to

←——————————————————————————————————

Figure 8

$\Lambda(c)$ and b, as well as the wind input and source terms, as found in Banner & Morison's (2010) study under the assumption of negligible currents. (*a*) The measured breaking wave crest length spectral density $\Lambda(c)$ for period 1 and period 3 for $U_{10} = 12\text{m s}^{-1}$. The blue and green vertical arrows indicate the wave age of the spectral peaks for period 1 and period 3 with associated speeds 11.0 and 15.5 m s^{-1}, respectively. (*b*) The modeled variation of the spectral density of breaking crest length per unit area and breaking strength for the spectral peak waves. (*c,d*) The developing seas' source term balance for period 1 (*c*) and period 3 (*d*). (The interested reader is referred to Banner & Morison 2010 for additional information.) Figure redrawn from Banner & Morison (2010, figures 8 and 9).

the moment when the free surface impinges another part of the free surface, these methods have been used to study primarily the onset of wave breaking.

The first serious validation of a breaking-wave simulation using a MEL method was provided by Dommermuth et al. (1988), who showed that their numerical solution for a breaking focusing wave group compared reasonably well with laboratory measurements of the surface elevation as well as the horizontal and vertical velocities using a laser anemometer. A more detailed comparison of velocity measurements via PIV was provided by Skyner (1996), who used a MEL model of Dold & Peregrine (1986) to simulate a plunging breaking wave. Although a phase discrepancy was observed near wave breaking, less than a 2% difference in the velocity comparison was attained by shifting the wave profiles to match the phase. The same numerical model has been used by Song & Banner (2002) to develop a criterion of wave breaking for focusing wave groups, encouraged by the previous work of Banner & Tian (1998) for modulating wave groups. The criterion developed numerically by Song & Banner (2002) has been confirmed experimentally by Andonowati et al. (2006) and Tian et al. (2008), demonstrating that it could be used as a predictive quantity for the onset of wave breaking. This indicates indirectly the usefulness of the MEL methods at the early stage of wave breaking.

Fochesato et al. (2007) studied numerically the 3D breaking of directional focusing waves using a higher-order MEL method combined with a fast multipole algorithm. Once a focused wave was created, the authors found that the subsequent overturning and breaking processes were locally quasi-2D, with weak transverse velocity and acceleration components. Conversely, they found that the wave kinematics beneath a breaking wave was different from that of a nonbreaking wave. For example, the horizontal velocity depended weakly on water depth. Although the development of the free surface during focusing and overturning was similar to observations, no comparison of numerical solutions with laboratory experiments has been made for 3D breaking waves.

Irisov & Voronovich (2011) examined breaking criteria in a random wave field of surface gravity waves using a MEL method. Through Monte-Carlo simulations, they found that locations of wave breaking correlated well with those of the maximum convergence of surface currents induced by long waves and therefore concluded that wave-breaking events take place mainly because of the decreasing length of relatively short waves by longer waves.

One of the shortcomings of the MEL method in modeling ocean waves of many wave components is that it is unable to resolve a wide range of spatial scales with a finite number of Lagrangian points. With increasing interest focused on rogue waves in random ocean wave fields, the accurate prediction of their occurrence has become paramount, in particular, for a relatively large area. Recently, a pseudospectral method developed originally by West et al. (1987) and Dommermuth & Yue (1987) has been found suitable for simulations of broadband ocean waves when combined with efficient fast Fourier transforms. It has been shown to simulate reliably the evolution of nonlinear irregular wave fields when compared with laboratory experiments (Grue et al. 2003, Goullet & Choi 2011). The method has been further developed by Craig & Sulem (1993) by reformulating the water wave problem in terms of the Dirichlet-Neumann operator (making the connection between Dirichlet and Neumann data), which in turn can be expanded in wave steepness to recover the formulation of West et al. (1987). As these pseudospectral methods are based on asymptotic expansion, they could be useful to study the onset of wave breaking but fail to simulate overturning waves.

For 2D breaking waves, an alternative approach without expanding the Dirichlet-Neumann operator in wave steepness is available. After mapping a physical domain under the free surface into a strip of finite thickness (in which the Dirichlet-Neumann operator can be easily defined), one can obtain a closed system of explicit nonlinear evolution equations for the surface elevation and the free surface velocity potential (Ovsjannikov 1974, Dyachenko et al. 1996, Chalikov & Sheinin 2005). As the free surface is parameterized by a conformal coordinate, the system in principle can

describe an overturning wave. This original formulation was due to Ovsjannikov (1974), but it was Chalikov & Sheinin (2005) who first simulated successfully an overturning wave. Babanin et al. (2007, 2010) used this numerical method to study the role of wind forcing, modeled as an external pressure, on the evolution of steepness, skewness, and asymmetry of a steep wave profile, but they stopped their simulations when the free surface became vertical. They also performed laboratory experiments, but the comparison between numerical solutions and laboratory measurements was only qualitative. Although this approach solves the Euler equations without imposing the small steepness assumption, it is limited to 2D waves due to a conformal mapping technique adopted for the derivation of the system of evolution equations.

6.2. Viscous Computations of Breaking Waves

Because of the difficulty of resolving small-scale free surface turbulence induced by wave breaking, only a small number of viscous simulations of breaking waves are currently available. In fact, most are limited to the evolution of a periodic wave train in relatively low–Reynolds number 2D flows (Chen et al. 1999, Song & Sirviente 2004, Iafrati 2009) although some 3D simulations have been attempted recently (Wang et al. 2009, Weymouth & Yue 2010).

Chen et al. (1999) studied a wave train with a plunging breaker using the volume of fluid method with a density ratio of 10^{-2}, a viscosity ratio of 0.4, a Bond number of 10^4, and a Reynolds number of 10^4. The exponential decay rate of the wave amplitude due to viscosity was estimated to be 1.9×10^{-2} based on linear theory but was found to increase to 0.16 during the active breaking process when the decay rate of the total energy was monitored numerically. One of their findings was that more than 80% of the prebreaking energy was dissipated within the first three wave periods following breaking. Although the physical parameters chosen for numerical simulations differ from those for the air-water system, this observation is consistent with the experimental measurements of Rapp & Melville (1990). Using a coupled level set and volume-of-fluid method, Wang et al. (2009) repeated the simulation of Chen et al. (1999) with the same computational setup and found good qualitative agreement between the two simulations.

Chen et al. (1999) also compared their direct numerical simulations with inviscid numerical solutions via a MEL method with constant viscous terms suggested by Longuet-Higgins (1992). To the point of jet re-entry onto the forward surface, the two solutions were observed to compare well, with the difference in the maximum velocity being approximately 1%.

Iafrati (2009) simulated the breaking of 2D periodic waves with initial steepness over the range $ka = 0.2$–0.65. Using a Navier-Stokes solver for a two-fluid system combined with a level-set method to capture the interface, he examined the effect of breaking intensity on the resulting flow. Iafrati chose the Reynolds number to be 10^4, although the Weber number in the simulations corresponded to a wavelength of 30 cm, which corresponds to a Reynolds number of 4.4×10^5. The density ratio chosen was between that of air and water, but the viscosity ratio of 0.4 was much greater than that between air and water.

Iafrati's simulations showed that wave breaking occurred for $ka > 0.33$: spilling-type breaking between $ka = 0.33$ and 0.35 and plunging-type breaking for $ka > 0.37$. During the most energetic breaking process, it is difficult to measure experimentally the role of bubbles in energy dissipation, but numerical simulations were able to describe quantitatively the amount of air trapped and the degassing process. It was concluded that major energy dissipation occurs locally at the region of small bubbles generated by the fragmentation of the air cavity entrapped by the plunging jet. The scaling law for the amount of air entrapped as a function of the initial wave steepness was found, and the primary circulation induced by the breaking process scaled with the velocity difference between the wave crest and trough.

Even though viscous simulations are essentially the only theoretical means to investigate detailed breaking processes and numerous improvements in numerical methods have been made (Wang et al. 2009, Weymouth & Yue 2010), they still suffer from various numerical and modeling issues to resolve small-scale turbulence and bubbles resulting from wave breaking. Furthermore, numerical results are compared qualitatively with laboratory experiments, mostly, in terms of free surface profiles. Therefore, a more robust computational method along with careful validation with high-quality laboratory measurements on detailed breaking processes is still desirable.

6.3. Parameterization of Energy Dissipation due to Wave Breaking

It is still problematic to simulate detailed breaking processes using a Navier-Stokes solver over a large computational domain. Hence a simple wave-breaking model would be useful if it at least accounts for energy dissipation due to wave breaking.

To describe intermittent wave-breaking effects, Sullivan et al. (2004, 2007) developed a stochastic forcing model, which was incorporated into a large-eddy-simulation model to study the wave-current interaction problem. They represented the constant-stress boundary condition by a sum of randomly distributed compact impulses determined from field and laboratory measurements. Their focus was wave-breaking effects on near-surface currents in the oceanic boundary layer, but feedback to the evolution of nonlinear surface waves (and therefore the forcing model) was not included. Hence the stochastic forcing model cannot be used in breaking- and postbreaking-wave simulations.

An alternative, but simpler, approach was proposed by Tian et al. (2010). Instead of simulating the complete breaking process, they represented the net effect of wave breaking by parameterizing energy dissipation in terms of global flow variables and incorporated them into an inviscid wave model that solves the Euler equations. Using the linearized boundary-layer analysis presented by Ruvinsky et al. (1991), Tian et al. (2010) proposed a so-called eddy viscosity model and estimated an eddy viscosity using characteristic scales of breaking waves measured through laboratory experiments. A possible use of eddy viscosity for breaking waves was suggested earlier by Longuet-Higgins (1992), who reformulated Ruvinsky et al.'s (1991) analysis and remarked, "It is highly interesting to consider whether an analogous theory might be formulated for breaking waves, in which the molecular viscosity would be replaced by a turbulent eddy coefficient."

By estimating the energy dissipation rate in terms of timescales and length scales of breaking waves, Tian et al. (2010) estimated the eddy viscosity as

$$\nu_{eddy} = \alpha H_{br} L_{br} / T_{br},$$

where T_{br} is defined as the time when the wave crest begins to fall to the time when the surface disturbance front is no longer obvious, L_{br} is the distance from incipient breaking to the location where the obvious surface disturbance ends, H_{br} refers to the falling crest height, and α is a proportional constant ($\alpha = 0.02$, as determined in Tian et al. 2010).

Tian et al. (2010) then estimated eddy viscosities associated with different wave groups using the experimental measurements and found them to depend on the breaking strength. Whereas the kinematic viscosity of water is $O(10^{-6}$ m^2 s^{-1}), the magnitudes of the eddy viscosity were found to be of the order of 10^{-3} m^2 s^{-1}, and the eddy viscosity increased as wave breaking intensified. For numerical simulations, the eddy viscosity model is applied in the region of active wave breaking during its time duration. When these estimates are used in the pseudospectral model, good agreement between numerical solutions and experimental measurements was found. **Figure 10** compares the spatial evolution of the total energy along the wave tank and of the temporal evolution of the surface elevation at three different wave-probe locations.
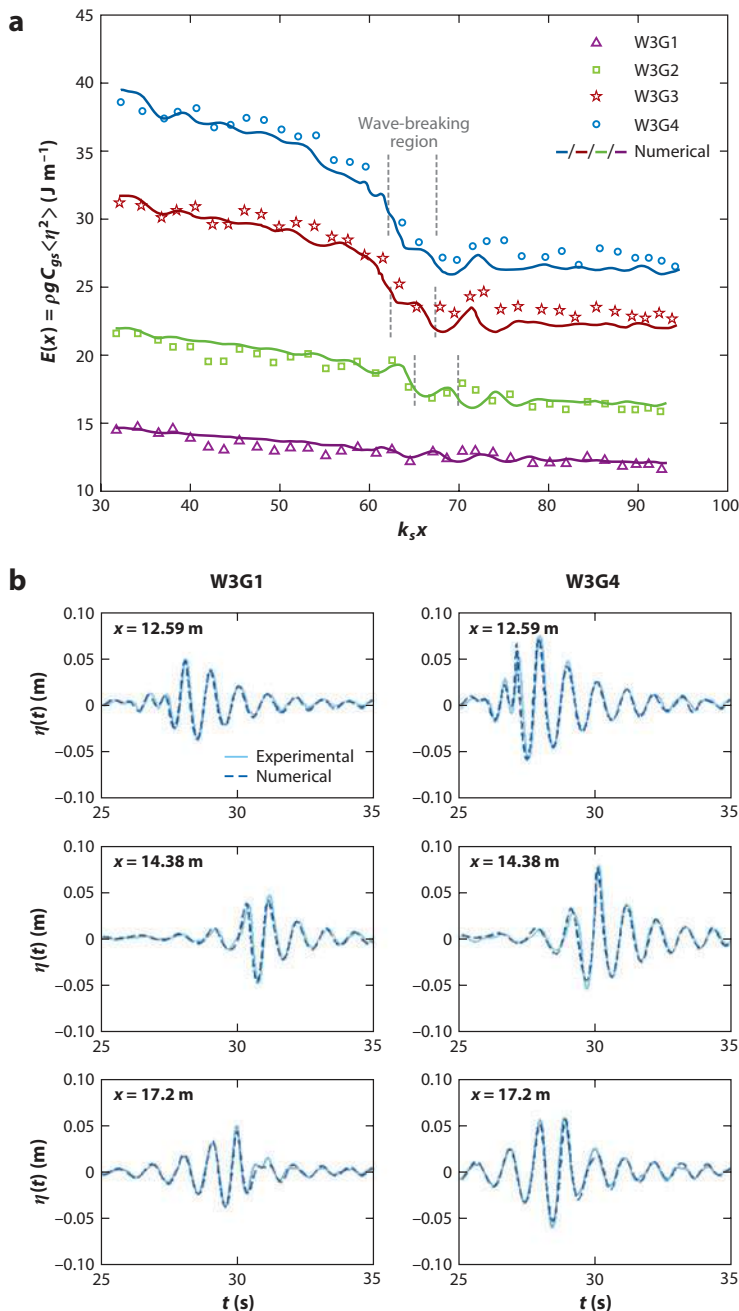
Even with such success, the original eddy viscosity model proposed by Tian et al. (2010) was limited for application to the simulation of evolving ocean waves as the time and location of wave breaking have to be known, and the eddy viscosity has to be estimated a priori through laboratory experiments, which is not realistic. Tian et al. (2012) proposed a solution to overcome this difficulty, suggesting formulae to estimate the temporal and spatial scales of wave breaking

through local wave characteristics:

$$k_b L_{br} = 24.3 S_b - 1.5; \quad \omega_b T_{br} = 18.4 S_b + 1.4; \quad k_b H_{br} = 0.87 R_b - 0.3;$$

where k_b, ω_b, S_b, and R_b are the local wave number, wave frequency, wave slope, and wave asymmetry, respectively, as defined in Tian et al. (2012), and are determined from the simulated wave profile. In addition, the critical wave slope beyond which wave breaking is predicted was chosen to be $S_C = 0.95$, where the local wave slope S is defined as $S = -\partial\zeta/\partial x$ with the minus sign introduced because the spatial derivative of the surface elevation is negative on the forward face of the wave crest. Tian et al. (2012) evaluated the applicability of the eddy viscosity model for three different wave groups: energy-focusing wave groups, wave groups subject to modulational instability, and irregular waves characterized by the JONSWAP spectrum. They found that the model predicts well the total energy dissipated in breaking waves and that the computed surface elevations following wave breaking agree satisfactorily with the measurements.

Although it has been shown that a simple eddy viscosity model can be useful, it has to be refined to perform better for various wave-breaking mechanisms and it must include a more robust criterion of breaking onset. In addition, the model needs to be developed for 3D breaking waves and should be validated carefully with laboratory experiments.

7. CONCLUDING REMARKS

In this review on breaking waves in deep and intermediate water depths, we focus on three physics-based areas in which we feel the most progress has been made over the past 20 years: the geometry of breaking, breaking-onset criteria, and dissipation due to breaking. We discuss the progress in three dimensions as well where appropriate. Additionally, field measurements and numerical simulations are discussed in some detail.

Regarding the geometry of breaking waves, many prior studies had focused on straightforward quantification of the wave's geometric properties, such as the limiting steepness, breaking crest asymmetry, and the evolution of breaking crest profiles, in an attempt to understand the fundamental physics of breaking waves. Recent progress has evolved to the point at which we can identify possible connections between the breaking crest geometry and the breaking-wave dynamics, i.e., energy dissipation and dissipation rate (e.g., Drazen et al. 2008; Tian et al. 2010, 2012). Additional work on this topic that considers the influence of three-dimensionality, wind forcing, and currents, for example, will lead to more significant contributions in the future.

The accurate prediction of wave-breaking onset remains a challenge; however, it too has progressed recently. Based on the parameters used, onset prediction can be classified into three categories: geometric, kinematic, and dynamic. Dynamic criteria based on local wave-energy growth rate appear robust, consistent with the available experimental evaluations. However, the application of the criteria in the phase-resolving, deterministic prediction of the evolution of nonlinear wave fields may be limited, as the calculation of the diagnostic parameter $\delta(t)$ is nontrivial.

During the past two decades, the determination of the energy dissipation, as well as its spectral distribution and the dissipation rate due to wave breaking, has been the focus of many investigations. The parameterization of the breaking-wave dissipation rate has benefited significantly from laboratory and field experiments. In fact, the combined effort has made available relationships among the three physics-based areas of breaking waves, i.e., links among the dynamics and the kinematics (e.g., $\varepsilon \sim \rho C^5/g$) and the parameterization of the dynamics using geometric properties [e.g., $b \sim S_b$ and $b \sim (hk)^{5/2}$].

It is evident from the discussions in Section 5 that field work on offshore breaking waves continues, although much remains to be done. Advances have been made in various areas, but

consensus among researchers is limited. In fact, few studies have been completed. The slow rate of progress is a result of the difficult nature of measurements in the field, as well as the costs associated with conducting these experiments.

Section 6 presents a focused discussion of the numerical progress on breaking-wave research. At this juncture, direct numerical simulations are not a viable option for ocean wave calculations over a large domain; therefore, a simpler approach should be adopted to model the breaking effects. This is explored using a simple eddy viscosity model, and when it is combined with an inviscid wave evolution model, the numerical results for the total energy dissipation and the surface elevation show good agreement with laboratory measurements of 2D breaking-wave experiments. Nevertheless, a more sophisticated theoretical model describing the interaction between breaking waves and turbulent flow fields is still necessary. In particular, it would be beneficial for 3D wave breaking, for which detailed experimental measurements are extremely difficult to obtain.

Overall, investigators continue to chip away at the difficult problem of quantifying wave breaking through laboratory investigations, field measurements, and numerical simulations. As this research area includes three of the most challenging problems in fluid mechanics (turbulence, two-phase flow, and interfacial flow), it is likely that progress will continue at a very slow pace.

DISCLOSURE STATEMENT

The authors are not aware of any biases that might be perceived as affecting the objectivity of this review.

ACKNOWLEDGMENTS

LITERATURE CITED

Agrawal EC, Terray EA, Donelan MA, Hwang PA, Williams AJ III, et al. 1992. Enhanced dissipation of kinetic energy beneath surface waves. *Nature* 259:219–20

Alves JH, Banner ML. 2003. Performance of a saturation-based dissipation-rate source term in modeling the fetch-limited evolution of wind waves. *J. Phys. Oceanogr.* 33:1274–98

Andonowati, Kusumawinahyu W, van Groesen E. 2006. A numerical study of the breaking of modulated waves generated at a wave maker. *Appl. Ocean Res.* 28:9–17

Babanin AV, Chalikov D, Young IR, Savelyev I. 2007. Predicting the breaking onset of surface water waves. *Geophys. Res. Lett.* 34:L07605

Babanin AV, Chalikov D, Young IR, Savelyev I. 2010. Numerical and laboratory investigation of breaking of steep two-dimensional waves in deep water. *J. Fluid Mech.* 644:433–63

Babanin AV, Waseda T, Kinoshita T, Toffoli A. 2011. Wave breaking in directional fields. *J. Phys. Oceanogr.* 41:145–56

Baldock TE, Swan C, Taylor PH. 1996. A laboratory study of nonlinear surface waves on water. *Philos. Trans. R. Soc. Lond. A* 354:649–76

Banner ML, Gemmrich JR, Farmer DM. 2002. Multiscale measurements of ocean wave breaking probability. *J. Phys. Oceanogr.* 32:3364–75

Banner ML, Morison RP. 2010. Refined source terms in wind wave models with explicit wave breaking prediction. Part I. Model framework and validation against field data. *Ocean Model.* 33:177–89

Banner ML, Peirson WL. 2007. Wave breaking onset and strength for two-dimensional deep-water wave groups. *J. Fluid Mech.* 585:93–115

Banner ML, Peregrine DH. 1993. Wave breaking in deep water. *Annu. Rev. Fluid Mech.* 25:373–97

Banner ML, Phillips OM. 1974. On the incipient breaking of small scale waves. *J. Fluid Mech.* 65:647–56

Banner ML, Song JB. 2002. On determining the onset and strength of breaking for deep water waves. Part II: Influence of wind forcing and surface shear. *J. Phys. Oceanogr.* 32:2559–70

Banner ML, Tian X. 1998. On the determination of the onset of breaking for modulating surface gravity water waves. *J. Fluid Mech.* 367:107–37

Benjamin TB, Feir JE. 1967. The disintegration of wave trains in deep water. Part 1. Theory. *J. Fluid Mech.* 27:417–30

Bonmarin P. 1989. Geometric properties of deep-water breaking waves. *J. Fluid Mech.* 209:405–33

Chalikov D, Sheinin D. 2005. Modeling extreme waves based on equations of potential flow with a free surface. *J. Comput. Phys.* 210:247–73

Chang KA, Liu PLF. 1998. Velocity, acceleration and vorticity under a breaking wave. *Phys. Fluids* 10:327–29

Chaplin J. 1996. On frequency-focusing unidirectional waves. *Int. J. Offshore Polar Eng.* 6:131–37

Chen G, Kharif C, Zaleski S, Li J. 1999. Two-dimensional Navier-Stokes simulation of breaking waves. *Phys. Fluids* 11:121–33

Chiang WS, Hwung HH. 2007. Steepness effect on modulation instability of the nonlinear wave train. *Phys. Fluids* 19:014105

Craig W, Sulem C. 1993. Numerical simulation of gravity waves. *J. Comput. Phys.* 108:73–83

Dean GB, Stokes MD. 1999. Air entrainment processes and bubble size distributions in the surf zone. *J. Phys. Oceanogr.* 29:1393–403

Diorio JD, Liu X, Duncan JH. 2009. An experimental investigation of incipient spilling breakers. *J. Fluid Mech.* 633:271–83

Dold JW, Peregrine DH. 1986. Water-wave modulation. *Proc. 20th Int. Conf. Coastal Eng.*, pp. 163–75. Reston, VA: ASCE

Dommermuth DG, Yue DKP. 1987. Numerical simulations of nonlinear axisymmetric flows with a free surface. *J. Fluid Mech.* 178:195–219

Dommermuth DG, Yue DKP, Lin WM, Rapp RJ, Chan ES, Melville WK. 1988. Deep-water plunging breakers: a comparison between potential theory and experiments. *J. Fluid Mech.* 189:423–42

Donelan MA. 2001. A nonlinear dissipation function due to wave breaking. *Proc. Eur. Cent. Medium-Range Weather Forecasts Workshop Ocean Wave Forecast.*, pp. 87–94. Reading, UK: ECMWF

Drazen DA, Melville WK. 2009. Turbulence and mixing in unsteady breaking surface waves. *J. Fluid Mech.* 628:85–119

Drazen DA, Melville WK, Lenain L. 2008. Inertial scaling of dissipation in unsteady breaking waves. *J. Fluid Mech.* 611:307–32

Duncan JH. 1981. An experimental investigation of breaking waves produced by a towed hydrofoil. *Proc. R. Soc. Lond. A* 377:331–48

Duncan JH. 1983. The breaking and nonbreaking wave resistance of a two-dimensional hydrofoil. *J. Fluid Mech.* 126:507–20

Duncan JH. 2001. Spilling breakers. *Annu. Rev. Fluid Mech.* 33:519–47

Duncan JH, Philomen V, Behres M, Kimmel J. 1994. The formation of a spilling breaker. *Phys. Fluids* 6:2558–60

Duncan JH, Qiao H, Philomin V, Wenz A. 1999. Gentle spilling breakers: crest profile evolution. *J. Fluid Mech.* 379:191–222

Dyachenko AL, Zakharov VE, Kuznetsov EA. 1996. Nonlinear dynamics of the free surface of an ideal fluid. *Plasma Phys. Rep.* 22:916–28

Fochesato C, Grilli S, Dias F. 2007. Numerical modeling of extreme rogue waves generated by directional energy focusing. *Wave Motion* 44:395–416

Gemmrich JR, Banner ML, Garrett C. 2008. Spectrally resolved energy dissipation rate and momentum flux of breaking waves. *J. Phys. Oceanogr.* 38:1296–312

Goullet A, Choi W. 2011. A numerical and experimental study on the nonlinear evolution of long-crested irregular waves. *Phys. Fluids* 23:016601

Grue J, Clamond D, Huseby M, Jensen A. 2003. Kinematics of extreme waves in deep water. *Appl. Ocean Res.* 25:355–66

Hwang PA, Wang DW. 2004. An empirical investigation of source term balance of small scale surface waves. *Geophy. Res. Lett.* 31:L15301

Hwung HH, Chiang WS, Hsiao SC. 2007. Observations on the evolution of wave modulation. *Proc. R. Soc. A* 463:85–112

Iafrati A. 2009. Numerical study of the effects of the breaking intensity on wave breaking flows. *J. Fluid Mech.* 622:371–411

Irisov V, Voronovich A. 2011. Numerical simulation of wave breaking. *J. Phys. Oceanogr.* 41:346–64

Janssen PAEM. 1991. Quasi-linear theory of wind-wave generation applied to wave forecasting. *J. Phys. Oceanogr.* 21:1631–42

Johannessen TB, Swan C. 2001. A laboratory study of the focusing of transient and directionally spread surface water waves. *Proc. R. Soc. Lond. A* 457:971–1006

Kharif C, Giovanangeli J-P, Touboul J, Grare L, Pelinovsky E. 2008. Influence of wind on extreme wave events: experimental and numerical approaches. *J. Fluid Mech.* 594:209–47

Kiger KT, Duncan JH. 2012. Air entrainment mechanisms in plunging jets and breaking waves. *Annu. Rev. Fluid Mech.* 44:563–96

Kjeldsen SP, Myrhaug D. 1979. Breaking waves in deep water and resulting wave forces. *Proc. Annu. Offshore Technol. Conf.*, pp. 2515–22. New York: Am. Inst. Min. Metall. Petrol. Eng.

Kjeldsen SP, Vinje T, Myrhaug D, Brevig P. 1981. Kinematics of deep water breaking waves. *Proc. Annu. Offshore Technol. Conf.*, pp. 317–25. New York: Am. Inst. Min. Metall. Petrol. Eng.

Kleiss JM, Melville WK. 2011. The analysis of sea surface imagery for whitecap kinematics. *J. Atmos. Ocean. Technol.* 28:219–43

Komen GJ, Cavaleri L, Donelan M, Hasselmann K, Hasselmann S, Janssen PAEM. 1994. *Dynamics and Modelling of Ocean Waves*. Cambridge, UK: Cambridge Univ. Press

Kway JHL, Loh YS, Chan ES. 1998. Laboratory study of deep-water breaking waves. *Ocean Eng.* 25:657–76

Lamarre E, Melville WK. 1991. Air entrainment and dissipation in breaking waves. *Nature* 351:469–72

Longuet-Higgins MS. 1981. On the overturning of gravity waves. *Proc. R. Soc. Lond. A* 376:377–400

Longuet-Higgins MS. 1982. Parametric solutions for breaking waves. *J. Fluid Mech.* 121:403–24

Longuet-Higgins MS. 1992. Theory of weakly damped Stokes waves: a new formulation and its physical interpretation. *J. Fluid Mech.* 235:319–24

Longuet-Higgins MS, Cokelet ED. 1976. The deformation of steep surface waves on water. I. A numerical method of computation. *Proc. R. Soc. Lond. A* 350:1–26

Lowen MR, Melville WK. 1991. Microwave backscatter and acoustic radiation from breaking waves. *J. Fluid Mech.* 224:601–23

McLean JW, Ma YC, Martin DU, Saffman PG, Yuen HC. 1981. Three-dimensional instability of finite-amplitude water waves. *Phys. Rev. Lett.* 46:817–20

Melville WK. 1982. The instability and breaking of deep-water waves. *J. Fluid Mech.* 115:163–85

Melville WK. 1994. Energy dissipation by breaking waves. *J. Phys. Oceanogr.* 24:2041–49

Melville WK. 1996. The role of surface-wave breaking in air-sea interaction. *Annu. Rev. Fluid Mech.* 28:279–321

Melville WK, Matusov P. 2002. Distribution of breaking waves at the ocean surface. *Nature* 417:58–63

Melville WK, Veron F, White CJ. 2002. The velocity field under breaking waves: coherent structures and turbulence. *J. Fluid Mech.* 454:203–33

Meza E, Zhang J, Seymour RJ. 2000. Free-wave energy dissipation in experimental breaking waves. *J. Phys. Oceanogr.* 30:2404–18

Nepf HM, Wu CH, Chan ES. 1998. A comparison of two- and three-dimensional wave breaking. *J. Phys. Oceanogr.* 28:1496–510

New AL. 1983. A class of elliptical free-surface flows. *J. Fluid Mech.* 130:219–39

Oh SH, Mizutani N, Suh KD, Hashimoto N. 2005. Experimental investigation of breaking criteria of deep-water wind waves under stong wind action. *Appl. Ocean Res.* 27:235–50

Ovsjannikov LV. 1974. To the shallow water theory foundation. *Arch. Mech.* 26:407–22

Perlin M., He JH, Bernal LP. 1996. An experimental study of deep water plunging breakers. *Phys. Fluids* 8:2365–74

Perlin M, Schultz WW. 2000. Capillary effects on surface waves. *Annu. Rev. Fluid Mech.* 32:241–74

Phillips OM. 1985. Spectral and statistical properties of the equilibrium range in wind-generated gravity waves. *J. Fluid Mech.* 156:505–31

Phillips OM, Posner FL, Hansen JP. 2001. High range resolution radar measurements of the speed distribution of breaking events in wind-generated ocean waves: surface impulse and wave energy dissipation rates. *J. Phys. Oceanogr.* 31:450–60

Qiao H, Duncan JH. 2001. Gentle spilling breakers: crest flow-field evolution. *J. Fluid Mech.* 439:57–85

Ramberg SE, Griffin OM. 1987. Laboratory study of steep and breaking deep water waves. *J. Waterw. Port Coast. Ocean Eng.* 113:493–507

Rapp RJ, Melville WK. 1990. Laboratory measurements of deep water breaking waves. *Philos. Trans. R. Soc. Lond. A* 331:735–80

Reul N, Branger H, Giovanangeli JP. 1999. Air flow separation over unsteady breaking waves. *Phys. Fluids* 11:1959–61

Ruvinsky KD, Feldstein FI, Freidman GI. 1991. Numerical simulations of the quasi-stationary stage of ripple excitation by steep gravity-capillary waves. *J. Fluid Mech.* 230:339–53

Schultz WW, Huh J, Griffin OM. 1994. Potential energy in steep and breaking waves. *J. Fluid Mech.* 278:201–28

She K, Greated CA, Easson WJ. 1994. Experimental study of three-dimensional wave breaking. *J. Waterw. Port Coast. Ocean Eng.* 120:20–36

Skyner D. 1996. A comparison of numerical predictions and experimental measurements of the internal kinematics of a deep-water plunging wave. *J. Fluid Mech.* 315:51–64

Song C, Sirviente AI. 2004. A numerical study of breaking waves. *Phys. Fluids* 16:2649–67

Song JB, Banner ML. 2002. On determining the onset and strength of breaking for deep water waves. Part I: Unforced irrotational wave groups. *J. Phys. Oceanogr.* 32:2541–58

Stansell P, MacFarlane C. 2002. Experimental investigation of wave breaking criteria based on wave phase speeds. *J. Phys. Oceanogr.* 32:1269–83

Stokes GG. 1880. Appendices and supplement to a paper on the theory of oscillatory waves. *Math. Phys. Pap.* 1:219–29

Sullivan PP, McWilliams JC, Melville WK. 2004. The oceanic boundary layer driven by wave breaking with stochastic variability. Part 1: Direct numerical simulations. *J. Fluid Mech.* 507:143–74

Sullivan PP, McWilliams JC, Melville WK. 2007. Surface gravity wave effects in the oceanic boundary layer: large-eddy simulation with vortex force and stochastic breakers. *J. Fluid Mech.* 593:405–52

Thorpe SA. 1992. Bubble clouds and the dynamics of the upper ocean. *Q. J. R. Meteorol. Soc.* 118:1–22

Thorpe SA. 1993. Energy loss by breaking waves. *J. Phys. Oceanogr.* 23:2498–502

Tian Z, Perlin M, Choi W. 2008. Evaluation of a deep-water wave breaking criterion. *Phys. Fluids* 20:066604

Tian Z, Perlin M, Choi W. 2010. Energy dissipation in two-dimensional unsteady plunging breakers and an eddy viscosity model. *J. Fluid Mech.* 655:217–57

Tian Z, Perlin M, Choi W. 2011. Frequency spectra evolution of two-dimensional focusing wave groups in finite depth water. *J. Fluid Mech.* 688:169–94

Tian Z, Perlin M, Choi W. 2012. An eddy viscosity model for two-dimensional breaking waves and its validation with laboratory experiments. *Phys. Fluids* 24:036601

Toffoli A, Babanin A, Onorato M, Waseda T. 2010. Maximum steepness of oceanic waves: field and laboratory experiments. *Geophys. Res. Lett.* 37:L05603

Touboul J, Giovanangeli JP, Kharif C, Pelinovsky E. 2006. Freak waves under the action of wind: experiments and simulations. *Eur. J. Mech. B* 25:662–76

Tsai W, Yue DKP. 1996. Computation of nonlinear free surface flows. *Annu. Rev. Fluid Mech.* 28:249–78

Tulin MP, Waseda T. 1999. Laboratory observations of wave group evolution, including breaking effects. *J. Fluid Mech.* 378:197–232

Wang Z, Yang J, Koo B, Stern F. 2009. A coupled level set and volume-of-fluid method for sharp interface simulation of plunging breaking waves. *Int. J. Multiphase Flow* 35:227–46

Waseda T, Kinoshita T, Tamura H. 2009. Evolution of a random directional wave and freak wave occurrence. *J. Phys. Oceanogr.* 39:621–39

West BJ, Brueckner KA, Janda RS, Milder DM, Milton RL. 1987. A new numerical method for surface hydrodynamics. *J. Geophys. Res.* 92:11803–24

Weymouth GD, Yue DKP. 2010. Conservative volume-of-fluid method for free-surface simulations on Cartesian grids. *J. Comput. Phys.* 229:2853–65

Wu CH, Nepf HM. 2002. Breaking criteria and energy losses for three-dimensional wave breaking. *J. Geophys. Res.* 107:3177

Wu CH, Yao A. 2004. Laboratory measurements of limiting freak waves on currents. *J. Geophys. Res.* 109:C12002

Yao A, Wu CH. 2004. Energy dissipation of unsteady wave breaking on currents. *J. Phys. Oceanogr.* 34:2288–304

Yao A, Wu CH. 2005. Incipient breaking of unsteady waves on sheared currents. *Phys. Fluids* 17:082104

Yao A, Wu CH. 2006. Spatial and temporal characteristics of transient extreme wave profiles on depth-varying currents. *J. Eng. Mech.* 132:1015–25

Young IR, Babanin AV. 2006. Spectral distribution of energy dissipation of wind-generated waves due to dominant wave breaking. *J. Phys. Oceanogr.* 36:376–94

Contents

Indexes

Errata

An online log of corrections to *Annual Review of Fluid Mechanics* articles may be found
at http://fluid.annualreviews.org/errata.shtml